

[Click here to view linked References](#)

Preserved organic matter in a fossil Ocean Continent Transition in the Alps: the example of Totalp, SE Switzerland

Tsvetomila Mateeva¹ *, George A. Wolff¹, Gianreto Manatschal², Suzanne Picazo³, Nick J. Kusznir¹ and John Wheeler¹

*mateeva@liv.ac.uk

¹Department of Earth, Ocean and Ecological Sciences, University of Liverpool, Liverpool, L69 3BX, UK

² CNRS-IPGS-EOST, Université de Strasbourg, 1 rue Blessig, F-67084 Strasbourg, France

³ University of Lausanne, 1015 Lausanne, Switzerland

Key words: serpentinization, organic matter, Totalp unit, biogeochemistry, ocean continent transition (OCT),

Abstract:

Evidence from ultraslow spreading mid-ocean ridges and both fossil and present-day Ocean-Continent Transitions (OCT) demonstrates that mantle serpentinization resulting from the interaction of mantle rock and water during tectonic exhumation is widespread. Observations at white smokers in modern ocean settings suggest that methane produced by serpentinization can support methanotrophic bio-systems, which use methane as the only source of carbon. An important question is whether such bio-systems are more generally pervasive in their association with serpentinized mantle in the subsurface. In this study, we examined whether there is evidence for such a methanotrophic system in exhumed serpentinized mantle at a magma-poor rifted continental margin, by probing for characteristic biological markers in these and associated sedimentary rocks in the Totalp unit of SE Switzerland. This unit represents a remnant of the former OCT of the southern Alpine Tethyan margin and was chosen because of its mild Alpine tectonic and low-grade metamorphic overprint during Alpine orogeny, hence giving potential for the preservation of indigenous organic matter (OM).

Totalp samples are characterized by low organic carbon contents of 11 to 647 ppm. The majority of the samples contain hydrocarbons in the form of *n*-alkanes in the range C₁₇ - C₃₆. Some

1 sediments contain isoprenoids, for example pristane and phytane and a suite of steranes that are
2 consistent with a marine origin for the OM preserved in the rocks. Traces of marine planktonic
3 and bacterial OM are preserved in the serpentinized mantle and overlying sediments of this
4 ancient Tethyan OCT, but there is no evidence that the OM has been generated from
5 methanotrophic bio-systems.
6
7
8
9
10

11 34
12
13

14 35 1. Introduction

15
16

17 Serpentinization is an important metamorphic exothermic hydration process potentially
18 contributing chemical energy for anaerobic life, as well as thermal energy at oceanic
19 hydrothermal vents (*e.g.* Shock et al. 2002; Jamtveit and Hammer 2012). Serpentinization
20 converts olivine and pyroxene to serpentine, other Fe-Mg minerals (magnetite, brucite, talc)
21
22
23
24
25
26
27
28
29
30
31
32
33
34
35
36
37
38
39
40
41
42
43
44
45
46
47
48
49
50
51
52
53
54
55
56
57
58
59
60
61
62
63
64
65

30 Serpentinization is an important metamorphic exothermic hydration process potentially
31 contributing chemical energy for anaerobic life, as well as thermal energy at oceanic
32 hydrothermal vents (*e.g.* Shock et al. 2002; Jamtveit and Hammer 2012). Serpentinization
33 converts olivine and pyroxene to serpentine, other Fe-Mg minerals (magnetite, brucite, talc)
34 and free molecular hydrogen (Eq. 1). The Mg component of olivine may hydrate as follows:
35
36
37
38
39
40
41
42
43
44
45
46
47
48
49
50
51
52
53
54
55
56
57
58
59
60
61
62
63
64
65



42 The Fe component of olivine contributes to forming Fe-Mg serpentine by an analogous reaction
43 and/or by reducing water



45 It has been proposed (*e.g.* McCollom 2013) that molecular hydrogen can then reduce CO₂
46 derived from carbonate and hydrogen carbonate in sea-derived pore waters to methane (CH₄)
47 at high pressure and temperature, via a Fischer-Tropsch-like reaction (Eq. 3).



49 Serpentinized mantle rocks exposed along slow to ultraslow-spreading Mid-Ocean Ridges
50 (MOR) show positive anomalies of methane and hydrogen in the overlying water column above
51 active tectonic zones (Rona et al. 1987; Charlou et al. 1988; Rona et al. 1992; Bougault et al.
52 1993; Charlou and Donval 1993; Charlou et al. 1998; Gràcia et al. 2000; Kelley and Shank

1 53 2010). The abiotically produced methane can be anaerobically oxidised by methanotrophic
2 54 bacteria using sulphate as the electron acceptor (Eq. 4).



8 56 Sulphate reducers are one of the dominant bacterial populations at hydrothermal vents
9

10 57 (McCollom and Shock 1997). Furthermore, methanotrophic bacteria have been identified at
11

12 58 Lost City (mid-Atlantic Ocean), a low-temperature alkaline hydrothermal vent supported by
13

14 59 energy derived from the formation of serpentinite (Hinrichs et al. 2000; Kelley et al. 2001;
15

16 60 Orphan et al. 2001; Kelley et al. 2005). Recently, bacterial anaerobic nitrate oxidation of
17

18 61 methane has been demonstrated in the laboratory (Haroon et al. 2013; Arshad et al. 2015), using
19

20 62 two different microorganisms (Raghoebarsing et al. 2006); this may also occur at the MOR
21

22

23 63 methane sources, but is likely to be a minor pathway as nitrate concentrations in seawater are
24

25

26 64 significantly lower than sulphate (μM vs. mM , respectively).

27

28

29

30

31 65 Recent studies have focussed on the relationship between serpentinization and organic
32

33

34 66 compounds, mainly methane in the laboratory (e.g. McCollom and Seewald 2013; Etiope and
35

36 67 Ionescu 2014), at present-day serpentinite-hosted hydrothermal vents (e.g. Kelley et al. 2005;
37

38 68 Delacour et al. 2008; Proskurowski et al. 2008), mud volcanoes (e.g. Mottl et al. 2003; Holm
39

40 69 et al. 2006), and exhumed serpentinite mantle domains with high H_2 concentrations and high
41

42

43 70 pH (e.g. Cardace et al. 2013). High concentrations of OM found at the Mid-Atlantic Ridge
44

45

46 71 (MAR; 4-6°N) were associated with serpentinitized peridotite rather than with the hydrothermal
47

48

49 72 vents (Ménez et al. 2012).

50

51

52 73 Hence, the present study uses an organic geochemical approach to quantify OM in the exhumed
53

54 74 mantle from an OCT in order to better understand the relationship between OM and mantle
55

56 75 serpentinization. We selected the Totalp unit exposed in the Eastern Swiss Alps, which
57

58

59 76 represents a remnant of the fossil Tethyan OCT emplaced during the Alpine orogeny (Fig. 1a)

60

61

62

63

64

65

1 (Bernoulli et al. 1985, Manatschal et al. 2003, Picazo et al. 2013). We searched for biomarkers
2 or molecular remains of former living organisms, specifically hydrocarbons with an origin
3 consistent with anaerobic methane oxidation (*e.g.* crocetane; Blumenberg et al. 2004). A wider
4 suite of biomarkers was used to determine source and thermal maturity of OM preserved in the
5 rocks.
6
7
8
9
10

11 82
12
13
14

15 83 **2. Regional geological setting of the Totalp unit** 16

18 84 The Totalp unit is located north of Davos in SE Switzerland. It is part of the Tethyan OCT (Fig.
19
20 85 1b). The peculiarity of the Totalp unit is that it experienced little Alpine deformation and only
21
22 86 a low grade Alpine metamorphic overprint, not exceeding 100-150°C, i.e. prehnite-pumpellyite
23
24 87 grade (Peters 1968; Früh-Green et al. 1990). The Totalp unit consists of two Alpine tectonic
25
26 88 units namely the Upper and Lower Ultramafic Totalp sub-units (*e.g.* Picazo et al. 2013). These
27
28 89 are mainly composed of serpentinized peridotite exhumed at the seafloor during Jurassic times
29
30 90 and ophicalcites that occur at the top basement; they can be found re-worked into the overlying
31
32 91 Jurassic marine sediments (Fig. 1c). In addition, the primary contacts between the exhumed
33
34 92 serpentinized mantle, the ophicalcites and the oceanic sediments are well-preserved (Weissert
35
36 93 and Bernoulli 1985).

43 94 2.1 Pre-Alpine and Alpine geological and thermal history

44
45 95 The serpentinized peridotites of the Totalp unit were exhumed to the Jurassic seafloor during
46
47 96 final late Middle Jurassic rifting (Peters and Stettler 1987; Bernoulli et al. 2003). Later, during
48
49 97 the Alpine orogeny, the exhumed mantle rocks were first tectonically emplaced within a Late
50
51 98 Cretaceous E-W directed nappe stack before being thrusted during the Tertiary collision over
52
53 99 the European units forming the present-day Alpine orogen (Weissert and Bernoulli 1985; Früh-
54
55 100 Green et al. 1990; Manatschal et al. 2003). The serpentinized peridotites in Totalp are

56
57
58
59
60
61
62
63
64
65

101 interpreted as derived from fertile subcontinental lithospheric mantle (Manatschal et al. 2001;
1
102 Müntener et al. 2010; van Acken et al. 2010), similar to other described remnants of fossil OCTs
2
103 from the Alps (*e.g.* Platta; Desmurs et al. 2002; Malenco in the Italian Alps; Müntener et al.
3
104 2004). Extensional faults and unroofing of their footwalls are responsible for the mantle
4
105 exposure at the seafloor (Picazo et al. 2013).

106

107 2.2 Lithologies

108 The Totalp unit consists mainly of serpentinized peridotites, ophicalcites and post-rift
109 sediments (Figs. 1 and 2; Table 1). This association is typical of an OCT across magma-poor
110 margins where magmatic rocks are often either very rare or absent. Three types of serpentinized
111 mantle rocks were identified:

- 112 i. Massive serpentinized peridotites, which preserve mantle textures and mainly
113 consist of serpentinized spinel-lherzolite. Locally these rocks also contain
114 pyroxenite and amphibole- and chlorite-rich layers (Picazo et al. 2013).
- 115 ii. During exhumation, the serpentinized peridotites are affected by localization of the
116 deformation and intensive fluid circulation leading to complete serpentinization of
117 fault-rocks, including serpentinite gouges, serpentinite cataclasites and foliated
118 cataclasites (Picazo et al. 2013). These rocks are best exposed in the Obersasställi
119 area, and they occur in the uppermost 150 m of the exhumed mantle in the footwall
120 of a Jurassic extensional detachment fault (Figs. 1 and 2; Picazo et al. 2013).
- 121 iii. Veins of serpentine that have been interpreted to result from later serpentinization
122 during low-grade Alpine metamorphism, as suggested by the oxygen isotopes (Früh-
123 Green et al. 1990). Some serpentine veins may result from the percolation of
124 meteoric water associated with regional metamorphism (Burkhard and O'Neil
125 1988).

126 Ophicalcites are complex rocks that are made of serpentinite and calcite and represent the result
1
127 of different processes (Bernoulli and Weissert 1985; Lemoine et al. 1987). They either result
2
128 from the total to partial *in-situ* replacement of serpentine by carbonate, tectonic processes
3
129 related to exhumation and hydrothermal systems, and/or cementation and filling of fractures by
4
130 sediments (*e.g.* neptunian dykes of Bernoulli and Jenkyns 2009). These processes occur at or
5
131 near the seafloor and are often associated with hydrothermal fluid circulation at temperatures
6
132 of 100-150°C (Früh-Green et al. 1990; Picazo et al. 2013). Most ophicalcites are formed under
7
133 static (non tectonic) conditions within 20 m of the paleo-seafloor (Picazo et al. 2013).
8
134 Sedimentary ophicalcites at Totalp include neptunian dykes and debris-flows (Fig. 2). The
9
135 neptunian dykes are carbonate veins filled with pink or grey carbonate (pelagic sediments or
10
136 mechanically reworked cements), filling fractures in the exhumed mantle. These dykes are
11
137 typically located in the tectonized, serpentized peridotites forming the uppermost few meters
12
138 of the exhumed mantle (Bernoulli and Weissert 1985; Picazo et al. 2013). The second main
13
139 type, the tectono-sedimentary ophicalcites, include cemented clasts of serpentinite, gabbro and
14
140 continental basement (Manatschal and Bernoulli 1999; Bernoulli et al. 2003; Picazo et al. 2013).
15
141 The sediments overlying the ophicalcite are mainly pelagic deposits of Late Jurassic to Early
16
142 Cretaceous age, some of which have been reworked (most likely by ocean bottom currents)
17
143 (Weissert and Bernoulli 1985). Red shales are overlain by radiolarian cherts and grey micritic
18
144 limestones intercalated with claystones (*e.g.* Radiolarite Formation and Calpionella or
19
145 Aptychus limestone Formation of Weissert and Bernoulli 1985). The top of the sequence is
20
146 formed by black siliceous shales that are characteristic of poorly oxygenated bottom waters
21
147 during the Early Cretaceous (Weissert et al. 1985; Weissert and Bernoulli 1985).
22
148 North east of Totalp, exposed on a topographic cliff near Gotschnagrat (Figs. 1 and 2), is a
23
149 weathered outcrop with visible pyrite on the top of the radiolarian cherts and siliceous
24
150 claystones (Fig. 3; Weissert and Bernoulli 1985). This outcrop has been described by Früh-
25
26
27
28
29
30
31
32
33
34
35
36
37
38
39
40
41
42
43
44
45
46
47
48
49
50
51
52
53
54
55
56
57
58
59
60
61
62
63
64
65

151 Green et al. (1990) as a zone of pyrite mineralization associated with radiolarian cherts. The
152 radiolarites contain quartz, illite, hematite and chlorite (Weissert and Bernoulli 1985). The
153 sulphidized outcrop has a bulk chemistry different from its surrounding and could have been
154 formed during early diagenesis or metasomatism of amorphous silica or limestone (Berner
155 1984; Williams et al. 1985). Alternatively, the sulphide could be related to a fossil
156 hydrothermal system (e.g. Styrt et al. 1981, Beard and Hopkinson 2000; Zeng et al. 2015). Early
157 diagenetic reactions producing pyrite depend inter alia on a source of OM as electron donor
158 (Fig. 3b); the high present-day porosity of the rock (Fig. 3c) could be produced by weathering
159 of calcite (Berner 1984). Hydrothermal vent systems are characterized by pelagic sediment
160 accumulation alongside ferrous oxides (*i.e.* radiolarian chert) of hydrothermal origin which can
161 potentially be preserved (Haymon 1989; Montgomery and Kerr 2009). The second most
162 common mineral in the sulphide bearing samples is quartz that may have originated from
163 amorphous silica or opal, which are common in hydrothermal vents (e.g MAR- mount Saldanha
164 36.30N; Dias and Barriga 2006; 25°48'N Rona 1984, 24°21'N; Rona 1984 ; Kane 23°35'N
165 Fracture zone; Kelley and Delaney 1987) reflecting a large input of hydrothermal silica (Dias
166 and Barriga 2006). There is no evidence of fossilized worm tubes associated with the zone of
167 pyrite mineralization; these are characteristic of inactive white smokers (Haymon 1983) and so
168 the origin of this formation remains unclear.
169

46 170 3. Sample Collection, Preparation and Analysis

48 171 3.1 Sample collection

51 172 A total of 47 samples were selected from the Totalp unit for geological and organic
52 geochemical studies (Table 1). We collected samples from the three main lithologies:
53 173 serpentinized mantle rock (lizardite, serpentinite gouge and cataclasite), ophicalcites (neptunian
54 174 dykes and tectono-sedimentary breccias) and associated sediments (Figs. 1 and 2; Table 1).
55
56
57
58
59
60
61
62
63
64
65

176 Samples were oriented, geo-referenced and collected using a geological hammer or a hand drill
1
177 using water as lubricant. On collection the samples were wrapped in pre-combusted foil
2
178 (400°C) for return to the laboratory.
3
179
4
180 3.2. Sample preparation
5
181 In order to avoid contamination with modern material the samples were cleaned with de-ionised
6
182 water ($18 \text{ M}\Omega \text{ cm}^{-1}$ resistivity; Milli-Q) and rinsed with re-distilled dichloromethane (DCM).
7
183 The outer edges were removed from each sample, which was then cut into smaller pieces using
8
184 a small rock saw lubricated with water. The aim was to get fresh, un-weathered samples for
9
185 laboratory analysis. These were then used for preparing thin sections and for stable isotope
10
186 analyses of carbonate veins, with 90 - 110 μg of calcite being extracted from using a small
11
187 electrical hand drill. For organic geochemistry selected pieces were washed with Milli-Q water
12
188 and DCM, then crushed (to particles $<50\mu\text{m}$) using a tungsten Tema Mill, which was previously
13
189 thoroughly cleaned (Decon-90 solution 2% v/v, milli-Q water, methanol and finally DCM). In
14
190 order to assess lab contamination, blanks composed of pre-combusted silica gel (600°C) were
15
191 subjected to the same procedures as the samples.
16
192
193 3.3 Mineralogical analyses
194 Optical microscopy, cathodoluminescence microscopy (CL; CITL Mk5-2) and X-Ray
195 Diffraction (XRD) were used to identify the mineralogy, chemistry, texture and textural
196 relations within the samples and to associate the mineralogy with the OM. A Panalytical X'Pert
197 PRO XRD system (CuK^{α} radiation, 45 kV, 40 mA) was used to identify the volume proportions
198 of the minerals associated with serpentinization and the polytypes of the serpentine minerals.
199

200 3.4 Geochemical analyses

Analyses of total carbon (TC) and total organic carbon (TOC) were performed before and after
decarbonation (10% HCL, 25°C), respectively, using a Carlo Erba Instrument NC2500
elemental analyser.

Stable isotopic analyses of organic carbon were carried out on five samples of four different
lithologies, prepared using a “sealed tube” method and injecting the resulting CO₂ into a VG
Sira 10 dual-inlet mass spectrometer (Craig 1957; Frazer and Crawford 1963; Sofer 1980). The
standard error for analysis is ± 0.1‰. The isotope data was normalized to IAEA-CH7
calibration material and reported using the VPDB scale. Carbon and oxygen isotope
measurements on calcite were performed on material extracted from veins by conversion to
CO₂ using a VG SIRA 10 MS Isocarb (common acid bath). The carbon and the oxygen isotope
analyses are referenced to the VPDB standard with a standard error for each analysis of ± 0.1‰
(McCrea 1950; Craig 1957; Friedman and O'Neil 1977; Swart et al. 1991).

Soxhlet extraction was used to extract the bitumen from the powdered rocks using DCM:
methanol (24 h) (modified after Wolff et al. 1995). Full blank extractions were conducted in
parallel to identify any possible contamination. After evaporation of the solvent, the extracts
were re-dissolved and passed through short columns of alumina and sodium sulphate using
hexane as solvent to isolate the hydrocarbons. The eluent from the alumina column was re-
dissolved in hexane (50 µL) and analysed by gas chromatography (GC) and GC- mass
spectrometry (GC-MS).

For GC-MS we used a GC Trace 1300 and Thermoquest ISQMS single quadrupole fitted with
a split-splitless injector, GC column (DB-5MS non-polar 5% phenyl and 95% methyl silicone
stationary phase, 60m x 0.25mm i.d., film thickness 0.1µm) using helium as a carrier gas (2mL
min⁻¹). The GC oven temperature was programmed from 60°C to 170°C after 1 min at 6°C min⁻¹,
then from 170°C to 315°C at 2.5°C min⁻¹ and finally held at 315°C for 15 min. GC-MS was

1 carried out in full data acquisition mode, providing mass spectra of compounds eluting from 20
2 to 90 minutes; these were identified by comparison with the literature and with authentic
3 standards where available (PAHs - polynuclear aromatic hydrocarbons). 5 α (H)-Cholestane was
4 used as an external standard for quantification; response factors were assumed to be 1, hence
5 data are semi-quantitative. Data were processed using XCalibur 1.2 software
6 (ThermoScientific).

7
8
9
10
11
12
13
14 The mean carbon numbers, MC# (Peltzer and Gagosian 1989) and the carbon preference index
15 (CPI) of *n*-alkanes (Peters et al. 2005a) were calculated over the carbon number range C₁₆- C₄₀
16
17
18
19 (Eq. 5 and 6; Table 2).

20
21
22
23

24 234
25 235 $MC\# = \sum ([C_i] \times C_i) / \sum [C_i]$ (Eq 5)

26 236 where [Ci] = concentration of the *n*-alkane with Ci carbon number

27
28
29
30

31 237
32 238 $CPI = 0.5 \times \sum ([odd\ C_{21} - C_{35}] / \sum [even\ C_{20}-C_{34}] + [odd\ C_{23} - C_{37}] / \sum [even\ C_{22}-C_{36}])$
33
34 239 (Eq 6)
35

36 240
37

38 241 **4 Carbon and hydrocarbon distributions in the analysed lithologies**

39
40
41

42 The TOC and TC results are summarized in Table 2 and vary considerably. The TOC values
43 are low, while TC reflect carbonate contents. The stable isotopic composition of carbonate
44 varied from -0.78 to 1.86‰VPDB and -11.7 to -6.2‰VPDB for $\delta^{13}\text{C}$ and $\delta^{18}\text{O}$, respectively
45
46
47 (Table 2; Fig. 4). Five decarbonated samples (sample 1: neptunian dyke; samples 9 and 39:
48 reworked tectono-sedimentary ophicalcite; sample 19: limestone; sample 69: specimen from
49 the sulphide-rich outcrop) have similar values for $\delta^{13}\text{C}_{\text{VPDB organic}}$ of between -27.4 and -26.2
50
51
52
53
54
55
56
57 % (Table 2).

58

59

60

61

62

63

64

65

1 249 Hydrocarbons (HCs) identified in Totalp samples include *n*-alkanes, steranes, polynuclear
2 250 aromatic hydrocarbons (PAHs), hopanes and isoprenoids, namely pristane and phytane.
3

4 251 Samples of the same lithology do not necessarily have similar distributions of HCs (Table 2).
5

6 252 This may reflect the heterogeneity of the samples collected, for example in the relative amount
7 253 of carbonate, calcite veins and serpentinite clasts.
8

9 254 Aliphatic compounds (> C15), mainly in the form of *n*-alkanes dominate (Fig. 5a). The CPI
10 255 (carbon preference index) for the *n*-alkanes are in the range 1 ± 0.3 , except for two samples that
11 256 were visibly weathered, having CPI = 2.6 - 2.87, i.e. an odd over even ratio for the *n*-alkanes
12 257 confirming contamination from modern material, such as soil (e.g. Villanueva et al. 1997).
13

14 258 Steranes included 20R and 20S $\alpha\beta\beta$ isomers from C₂₇ to C₂₉, as well as 20 R and S diacholestane
15 259 and pseudohomologues (Fig. 5 b). The steranes were dominated by C₂₇ compounds with a lower
16 260 abundance of C₂₈ and C₂₉ pseudo-homologues (Fig. 5 b). The ranges of values for the thermal
17 261 maturity parameters of the C₂₇ steranes are between 0.41 and 0.69 for ST1 = $\alpha\alpha\alpha$ 20S/ $\alpha\alpha\alpha$ 20S+
18 262 $\alpha\alpha\alpha$ 20R and 0.37 and 0.59 for ST2 = $\alpha\beta\beta$ / $\alpha\alpha\alpha+\alpha\beta\beta$ (Fig. 6; Seifert and Moldowan 1980; Peters
19 263 et al. 2005b). PAHs having molecular masses ≤ 276 were identified in some of the bitumen
20 264 extracts (Table 2; Fig. 5 c).
21

22 265
23

24 266 4.1. Serpentinite
25

26 267 All serpentinite samples contain *n*-alkanes, and several PAHs in the form of phenanthrene (P)
27 268 and fluoranthene (Fluo); steranes and hopanes were largely absent (Table 2).
28

29 269
30 270 4.1.1 Upper ultramafic sub-unit
31

32 271 *Massive serpentinite*
33

34 272 The massive serpentinites collected from the Weissfluhjoch (samples 77, 78; Fig. 1c; Table 1)
35 273 area have HC concentrations between 0.05 to 4 ppm while the C₂₉ *n*-alkane dominates their
36

1 distribution ($C_{max}=29$; Table 2). Total carbon (454 ppm) and total organic carbon (TOC) (≈ 180
2 ppm) concentrations are both very low.
3
4
5
6
7 274
8 275
9 276
10 277
11 278
12 279
13 280
14 281
15 282
16 283
17 284
18 285
19 286
20 287
21 288
22 289
23 290
24 291
25 292
26 293
27 294
28 295
29 296
30 297
31 298
32 299
33 300
34 301
35 302
36 303
37 304
38 305
39 306
40 307
41 308
42 309
43 310
44 311
45 312
46 313
47 314
48 315
49 316
50 317
51 318
52 319
53 320
54 321
55 322
56 323
57 324
58 325
59 326
60 327
61 328
62 329
63 330
64 331
65 332

4.1.2 Lower ultramafic sub-unit

Massive serpentinite

XRD analysis shows a lizardite polytype 1 (Bailey 1969) (87%), garnet (andradite) (7%) and pyroxene (clinopyroxene) (5%). In thin section olivine is completely replaced by serpentine minerals, with phantoms of pyroxene, euhedral magnetite, spinel and several calcite and carbonate veins not visible to the naked eye (Table 1).

HC concentrations vary from 23 ppm for the serpentinite from Parsenfurgga (sample 5) to 900 ppm from an outcrop with ophicalcite in Obersasställi (sample 16; Fig. 1c; Table 2). The TOC values range from 102-176 ppm and TC from 395-3134 ppm; steranes and hopanes are below detection limits (BDL) (Table 2). Serpentinite samples showing numerous calcite veins (sample 24, 26, 44 and 47) have higher amounts of TC (20400 to 42500 ppm). They show variable TOC (19 to 135 ppm) and low HC concentrations (1- 124 ppm). In the lower ultramafic sub-unit a red coloured serpentinite was identified by XRD to contain hematite (4%) (Table 1). The serpentine mineral is a lizardite polytype 1 (59%), also containing talc (18%) and calcite (19%). The isotopic composition of the calcite in the veins is 0.03‰ and -11.75‰ for $\delta^{13}\text{C}_{\text{VPDB}}$ and $\delta^{18}\text{O}_{\text{VPDB}}$, respectively (Fig. 4).

Serpentinite cataclasite and gouges

The serpentine cataclasites and gouges have TC of 540-875 ppm, *n*-alkanes with a carbon number range of C₁₇-C₃₆ and no detectable steranes or hopanes (Table 1 and 2). The serpentine cataclasites (sample 70), which are less deformed than the serpentine gouge (sample 69), contain more hydrocarbons (46 ppm and 3 ppm, respectively Table 2) but similar TOC contents (284 and 269 ppm, respectively).

299
1
2 300 4.2. Ophicalcite
3
4
5 301 The ophicalcites from the Totalp unit all contain *n*-alkanes and the PAHs (P, Fluo and Pyr, see
6
7 302 glossary; Table 2). Steranes and hopanes are also present in the majority of samples.
8
9
10 303
11
12 304 4.2.1. *Neptunian dykes*
13
14 305 Samples of neptunian dykes have a red micritic limestone matrix with millimetre-scale
15
16 306 serpentinite clasts and calcite veins (samples 1, 23) (Fig. 1c, Table 1). The $\delta^{13}\text{C}_{\text{VPDB}}$ organic of
17
18 307 one of the samples (sample 1) was - 27.1‰ (Table 2). There are high amounts of TC with
19
20 308 variable TOC (15 to 103 ppm) and HC concentrations (0.3 – 121 ppm) (Table 2).
21
22
23
24 309
25
26 310 4.2.2 *Tectono-sedimentary ophicalcites*
27
28
29 311 The tectono-sedimentary ophicalcite has various sub-lithologies from a reworked tectono-
30
31 312 sedimentary breccia with folded serpentinized and carbonate clasts in a red carbonate matrix
32
33 313 crosscut by calcite veins (sample 9) to centimetre scale serpentinite clasts in a carbonate vein
34
35 314 (sample 72) (Fig. 1c) (Table 1). The stable isotopic composition $\delta^{13}\text{C}_{\text{VPDB}}$ organic of one of the
36
37 315 samples was -26.1‰ (sample 9) (Table 2). A second type of ophicalcite, a serpentinite breccia
38
39 316 composed only of serpentinite clasts fragmented by calcite veins has low TOC (30 ppm) and
40
41 317 HCs concentrations (124 ppm) including only *n*-alkanes (sample 72) (Table 2). The isotopic
42
43 318 compositions of the calcite veins surrounding the serpentinite clast are 1.60‰ and -
44
45 319 10.6‰ VPDB for $\delta^{13}\text{C}$ and $\delta^{18}\text{O}$, respectively. The third most common ophicalcite is composed
46
47 320 of anhedral serpentinite clasts, carbonate veins, calcite veinlets in a reddish pelagic matrix and
48
49 321 has a low amount of TOC (11-116 ppm), but high concentrations of HCs (2-2470 ppm) (samples
50
51 322 21, 25, 39, 41, 42, 44, 66; Fig. 1c; Tables 1 and 2). The isotopic composition of the samples
52
53 323 varies from $\delta^{13}\text{C}_{\text{VPDB}} = 0.32\text{\textperthousand}$, $0.42\text{\textperthousand}$ and $0.58\text{\textperthousand}$ with $\delta^{18}\text{O}_{\text{VPDB}} = -11.75\text{\textperthousand}$, $-10.28\text{\textperthousand}$ and -

1 324 10.9‰ (for samples 25, 42 and 39 respectively) to $\delta^{13}\text{C}_{\text{VPDB}} = 1.07$ and 1.78‰ with $\delta^{18}\text{O}_{\text{VPDB}} =$
2 325 -11.7 to -7 ‰ for samples 42 (second generation calcite vein) and 41 (Fig. 4, Table 1). Isotopic
3 326 analysis of organic carbon (sample 39) gave $\delta^{13}\text{C}_{\text{VPDB organic}} = -27.4\text{\textperthousand}$ (Table 2). The ophicalcite
4 327 outcrop near the Gotschnagrat NE Totalp has isotopic values for calcite veins of 1.86‰ for
5 328 $\delta^{13}\text{C}_{\text{VPDB}}$ and -6.2‰ for $\delta^{18}\text{O}_{\text{VPDB}}$ (sample 66).
6
7
8
9
10
11
12
13
14
15
16
17
18
19
20
21
22
23
24
25
26
27
28
29
30
31
32
33
34
35
36
37
38
39
40
41
42
43
44
45
46
47
48
49
50
51
52
53
54
55
56
57
58
59
60
61
62
63
64
65

330 4.3. Sediments

331 Limestones are, together with radiolarian cherts, the most common sediments in the Totalp
332 unit. All of the sediment samples contain detectable levels of HCs including PAHs.

334 4.3.1 Radiolarian cherts

335 The radiolarian cherts are situated mostly around the Gotschnagrat NE Totalp (samples 62, 68)
336 and along small distributed outcrops some of which are 1-2 m in length and located between
337 Parsennfurgga and Parsenhütte (sample 6; Fig. 1c). Except for the weathered sample, they have
338 very low concentrations of HCs (1 -17 ppm) and low TOC values (66-187 ppm) (Table 2). The
339 radiolarian cherts are hard, fine grained siliceous sediments that are transected by post-
340 depositional quartz and calcite veins, the latter having isotopic compositions of $\delta^{13}\text{C}_{\text{VPDB}} = -$
341 0.79‰ and $\delta^{18}\text{O}_{\text{VPDB}} = -6.4\text{\textperthousand}$ (Sample 62; Table 1; Fig. 4).

343 4.3.2 Siliceous shales

344 The siliceous shales are located mostly above Parsenhütte and around the Gotschnagrat
345 (samples 15, 18, 60, 61; Fig. 1c). XRD analysis of the siliceous shales (sample 61) above the
346 pyrite rich area revealed a mineralogical composition consisting of quartz (83%), albite (10%),
347 pyrite (2%), illite/muscovite (4%), chlorite and hematite. This composition is similar to the
348 siliceous shale (samples 15, 18) found nearby, which consists of quartz (89%), plagioclases

1 349 (6%), illite/muscovite (4%), chlorite and trace of hematite (Fig. 1c; Table 1). They have low
2 350 concentrations of HCs (13 – 144 ppm) and variable amounts of TOC (194-433 ppm) (Table 2).
3
4 351 *4.3.3 Limestone*
5
6 352 Samples (53 to 57) are pelagic grey limestones that contain visible calcite veinlets and fine
7 353 greyish veinlets (serpentinite) from the syncline in the Parsennhütte (Fig.1c) (Table 1). They
8
9 354 contain a low amount of TOC (14-92 ppm) and variable concentrations of HCs (Table 2).
10
11
12 355 The pelagic limestones with higher amount of calcite veins (samples 10, 19) are also poor in
13 356 TOC (74- 82ppm) and contain HCs from 79 to 171 ppm (Fig. 1c; Tables 1 and 2). Isotopic
14 357 analyses of the first generation of calcite veins in sample 19 show $\delta^{13}\text{C}_{\text{VPDB}} = 0.56\text{\textperthousand}$ and
15
16 358 $\delta^{18}\text{O}_{\text{VPDB}} = -6.5\text{\textperthousand}$ and $\delta^{13}\text{C}_{\text{VPDB organic}} = -26.6\text{\textperthousand}$ (Fig. 4; Table 1).
17
18
19 359
20
21
22 360 *4.4 Silica – rich carbonate (sulphide-rich outcrop)*
23
24
25
26 361 The mineralogy of the pyrite rich rocks is dominated by calcite (53%) with quartz (24%),
27
28 362 chlorite (12%) and pyrite (6%) being the other main minerals (sample 63, 64, 65; Figs. 1c and
29
30 363 3; Table 1). The samples were on the top of the radiolarian chert and red shale sequences where
31
32 364 the contact between these rocks are weathered and not affected by deformation (Fig. 3). Isotopic
33
34 365 composition of organic carbon is $\delta^{13}\text{C}_{\text{VPDB organic}} = -26.02\text{\textperthousand}$ (sample 64) and that of the calcite
35
36 366 veins in the same sample 1.4% for $\delta^{13}\text{C}_{\text{VPDB}}$ and -6.6% for $\delta^{18}\text{O}_{\text{VPDB}}$ (Table 1). The samples
37
38 367 are characterized by a TOC contents from 153 to 647ppm and low HC concentrations (1 – 24
39
40 368 ppm) (Table 2); bitumen extracts are dominated by elemental sulphur, but HCs include *n*-
41
42 369 alkanes, PAHs (P, Fluo, MPs) and steranes (Table 2).
43
44
45
46
47
48
49
50
51
52 370
53
54
55 371 **5 Interpretation and discussion**
56
57
58
59
60
61
62
63
64
65

372 Traces of OM with a composition consistent with a marine origin were found in serpentinized
1
373 exhumed mantle. The generally low and variable amounts of TOC reflects the large lithological
2
374 diversity of the Totalp area, and the distributions of hydrocarbons are consistent with the
3
375 temperature history of the Totalp unit (*i.e.* no metamorphic overprint) (Table 2; Fig. 5).
4
5
6
7
8
9

10 376 5.1 Source of OM
11
12

13 377 A cross-plot of Pristane (Pr) to *n*-C₁₇ versus phytane (Ph) to *n*-C₁₈ is commonly used to
14
378 determine the depositional environment of OM in sedimentary rocks (Peters et al. 2005b). For
15
379 the Totalp samples (Fig. 7), this cross-plot implies a reducing (anoxic) depositional
16
380 environment for the OM, with a marine source of planktonic algal/bacterial OM consistent with
17
381 a marine mixed transitional environment that might be expected at this fossil OCT. Sterane
18
382 ternary diagrams are also commonly used to provide information on the source of OM in
19
383 sedimentary rocks (Peters et al. 2005a). Comparison of Totalp steranes with predicted
20
384 distributions of source materials (Fig. 8) are consistent with a mixed marine source of
21
385 planktonic algal and bacterial OM (Gonçalves et al. 2013; Wójcik-Tabol and Ślączka 2015) and
22
386 are similar to OM deposited in marine settings during and since the Jurassic (Grantham and
23
387 Wakefield 1988; Wójcik-Tabol and Ślączka 2015). Such a source for OM in the radiolarian
24
388 cherts reflects the dominant planktonic signature of coccoliths and nanoconids (Manatschal et
25
389 al. 2003). The variability in the sterane distributions most likely reflects spatial and temporal
26
390 variability in environmental conditions during OM deposition.
27
28
29

30 391 In five samples (ophicalcite, limestone and samples from the sulphide bearing outcrop) with
31
392 enough TOC to allow measurement of its stable isotopic composition, the determined values of
32
393 $\delta^{13}\text{C}_{\text{VPDB organic}}$ of *ca.* -26.2 to -27.4‰ (Table 2) are again consistent with an origin from marine
33
394 OM (-26‰ ± 7‰) (Schidlowski 1988; Hayes et al. 1990) and are similar to those found in
34
395 hydrothermal systems from the Galapagos ($\delta^{13}\text{C} = -27.4\text{\textperthousand}$) and the Guaymas Basin ($\delta^{13}\text{C} = -$
35
36
37
38
39
40
41
42
43
44
45
46
47
48
49
50
51
52
53
54
55
56
57
58
59
60
61
62
63
64
65

1 25‰ to - 21‰) (Orem et al. 1990). Orem et al. (1990) argued that the OM in these
2 hydrothermal systems derived from chemoautolithotrophic bacterial production. The carbon
3 isotopic composition of methane in modern hydrothermal vents ranges from -8.8 to -19.6‰ (

4 e.g. TAG 26°N -8/-9.5‰, Rainbow 36°14'N -15.8‰, see Charlou et al. 2002; Lost City 30°N
5 -13.6 to -8.8‰, Kelley et al. 2005; Bradley and Summons 2010). Fixation of hydrothermal
6 methane by methanotrophs would be expected to lead to OM more depleted in ^{13}C by 15 - 30‰
7 (Summons et al. 1994; Schidlowski 2001; Templeton et al. 2006), i.e. in the range -23.8 to -
8 34.6‰ assuming the most conservative fractionation. Hence, isotopic data from the Totalp
9 samples suggests that there could be a contribution from methanotrophic biomass; however the
10 values are also consistent with marine-derived OM. Taken together with the molecular data and
11 in the absence of specific methanotrophic biomarkers (e.g. crocetane), we consider that the
12 Totalp hydrocarbons derive from marine OM.

13 *5.1.1 Thermal history of OM*

14 The distributions of PAHs are in part consistent with a high temperature origin (e.g. Killops
15 and Massoud 1992), for example with pyrolytic residues (e.g. Geissman et al. 1967) arising
16 from OM alteration by hydrothermal activity (Kawka and Simoneit 1990) or low-grade
17 metamorphism (Heymann et al. 2003). Hence, the methyl-PAH/PAH ratios of ≤ 0.8 observed
18 in our samples are consistent with a pyrogenic source (Saha et al. 2009). However, the Fluo/Pyr
19 ratio < 0.6 of all the samples is lower than what would be expected of an exclusively pyrolytic
20 source and indicates that lower temperature pathways of PAH formation also contribute to the
21 HCs (Fabiańska et al. 2016). The biomarker maturation parameters of C₂₇ steranes fall within
22 values that might be expected within a temperature envelope consistent with a moderate thermal
23 history (Fig. 6; *ca.* 80 - 150°C; Mackenzie et al. 1980; Peters et al. 2005a) and are therefore
24 consistent with the temperature history of the basin (Früh-Green et al. 1990; Peters et al. 2005b).

25 This suggests that where steranes are present, their degree of isomerisation reflects gradual

1 maturation over time, rather than the pyrogenic process that may have yielded PAHs at the
2 contact of hot rock with seawater OM.
3
4

5 **422 5.1.2 Origin of calcite veins**
6

7
8 **423** The measured carbon and oxygen isotopic composition of carbonates are 0 to 2‰ and -11.7
9 to -6.2‰, for $\delta^{13}\text{C}_{\text{VPDB}}$ and $\delta^{18}\text{O}_{\text{VPDB}}$, respectively and are similar to values previously reported
10
11 for calcite veins in ophicalcite and late calcite veins collected in the Davos-Parsenn and Arosa
12 areas (Fig. 4; Früh-Green et al. 1990). The $\delta^{13}\text{C}_{\text{VPDB}}$ values are consistent with seawater-
13 derived early diagenetic calcite (Fig. 4a) (Hudson 1977; Coleman et al. 1993; Heydari 1997).
14
15 **428** The $\delta^{18}\text{O}_{\text{VPDB}}$ values of the calcite veins for the majority of samples vary between -11.7 to -
16 6.2‰ and indicate calcite precipitation during shallow burial (<250m), not influenced by
17 organic carbon derived CO₂ but typical of Cretaceous calcite (Dix and Mullins 1992; Heydari
18
19 1997). One sample (radiolarian chert) has a negative calcite carbon isotope value perhaps
20 indicating the influence of CO₂ delivered from diagenesis of OM (Heydari 1997).
21
22
23
24
25
26
27
28
29
30
31
32
33
34
35
36
37
38
39
40
41
42
43
44
45
46
47
48
49
50
51
52
53
54
55
56
57
58
59
60
61
62
63
64
65

433
434 **5.1.3 OM in serpentinite – mechanism of emplacement**
435
436
437
438
439
440
441
442
443

435 The occurrence of HC's in the serpentinite rocks of Totalp is at first sight surprising.
436 Schwarzenbach et al. (2013) listed the five main sources of organic carbon (OC) that can be
437 preserved in basement rocks, namely: seawater, mantle, Fischer-Tropsh-like reactions (F-T),
438 *in-situ* production from microbial activity in the basement rock, and, thermogenic
439 decomposition of OM. The hydrocarbons recovered from the Totalp serpentinites and the OC
440 have isotopic compositions consistent with an origin from marine OM, *i.e.* from a seawater
441 source rather than from *in-situ* production or abiotic F-T reactions. Therefore, the probable
442 origin of the OC preserved in the rocks is from dissolved and particulate organic carbon (DOC
443 and POC) derived from seawater or thermal alteration of OM in sediments that then migrated

1 444 to the basement rock within fluids (Fig. 9a). However, there could be different pathways of
2 445 emplacement of OM in the serpentinites.
3
4

5 446 The OM could have been deposited within the two types of precipitated carbonate found in the
6 447 serpentinite, namely the mechanically deposited carbonate that fills fractures, or *via* pore fluids
7
8 448 fuelling the formation of calcite veins (Fig. 9b; Bernoulli and Weissert 1985; Früh-Green et al.
9
10 449 1990). The latter has an isotopic composition consistent with seawater carbonate and any DOM
11
12 450 transported with the pore fluids would be trapped within the calcite matrix on precipitation
13
14 451 (Figs. 4 and 9b). The presence of ophicalcite and the numerous calcite veins from the time of
15
16 452 exhumation indicates a high supply of dissolved inorganic carbon (Ménez et al. 2012). As the
17
18 453 OM clearly has a marine origin, it could have been emplaced by the first main phase of fluid-
19
20 454 rock interactions at the ocean floor and the tectono-sedimentary and hydrothermal processes
21
22 455 described by Früh-Green et al. (1990). The OM may have migrated with seawater through
23
24 456 fractures in the sediment into the basement rock (Fig. 9c; Delacour et al. 2008). These fractures
25
26 457 formed by tectonic and crystallization stresses, which are not reliant on matrix permeability
27
28 458 (Farough et al. 2016). Where initial contact between DOM-containing fluid and rock was at
29
30 459 relatively high temperature, this could have led to the formation of the “pyrolytic” PAHs.
31
32

33 460 With respect to the sedimentary facies, organic carbon preservation is linked to grain size (or
34
35 461 mineral surface area) and oxygen exposure after deposition (Fig. 9d; Hartnett et al. 1998;
36
37 462 Kennedy et al. 2002). Clay minerals, one of the constituents of shale sediments found in the
38
39 463 Totalp unit, strongly retain DOM both on the external surfaces and interlayer spaces of clay
40
41 464 particles (Kennedy et al. 2002). However the Totalp sediments have low TOC values and could
42
43 465 been highly oxidised during deposition or diagenesis. During deposition of shales, OM is also
44
45 466 deposited as discrete biogenic particles, but largely these are not preserved; rather clays,
46
47 467 particularly smectites, facilitate the absorption of DOM and POM from seawater and pore-
48
49 468 fluids, and preserve it during burial (Kennedy et al. 2002).

1 469 In summary, OM in the exhumed mantle rocks at Totalp is of marine origin that migrated into
2 470 the serpentinite most likely from the overlying seawater or sediment cover (Simoneit et al.
3
4 471 1978; Simoneit and Philp 1982). Our results are consistent with previous studies that show a
5
6 472 lack of, or only minor formation of the CH₄ and H₂ needed for the production of OM involving
7
8 473 serpentinization at low-temperature (McCollom and Donaldson 2016) and that the molecules
9
10 474 necessary for life at hydrothermal systems are formed during the abiotic degradation of existing
11
12 475 OM at low temperatures on the ocean floor (Reeves et al. 2014).

13
14 476

15 477 **6 Conclusions**

16
17
18
19
20
21 478

22
23
24
25 479 We provide evidence for the preservation of traces of OM originally deposited in a reducing
26
27 480 marine environment in serpentized mantle rocks and overlying sediments, but with no
28
29 481 indication that the OM was generated from methanotrophic bio-systems. The presence of OM
30
31 482 within serpentized mantle raises two questions; how much is there and how is this OM
32
33 483 distributed in depth? Drilling to recover rock cores from the Totalp area would allow sampling
34
35 484 of serpentized mantle deeper than surface outcrops and would shed light on the depth
36
37 485 distribution of OM and its composition.

38
39 486

40 487 **Acknowledgments**

41
42
43
44
45
46
47 488 The Margin modelling program MM3 is acknowledged for funding. A. Thompson, S. Crowley,
48
49 489 S. Blackbird, G. Harriman, E. Fisher, J. Utley, N. Carr and S. Petev are thanked for scientific
50
51 490 and technical assistance. Two anonymous reviewers are thanked for their helpful comments
52
53 491 that improved the manuscript.

54
55
56
57 492

58 59 493 **Figure and Table Legends**

60
61
62
63
64
65

494
1 Fig. 1 Maps showing location and geology of the Totalp area. **a** Location of the Totalp area
2 in the tectonic map of the Alps (from Schmid et al. 2004; modified by Mohn et al. 2010).
3
4
5
6
7
8
9
10
11
12
13
14
15
16
17
18
19
20
21
22
23
24
25
26
27
28
29
30
31
32
33
34
35
36
37
38
39
40
41
42
43
44
45
46
47
48
49
50
51
52
53
54
55
56
57
58
59
60
61
62
63
64
65

495
496
497
498
499
500
501
502
503
504
505
506
507
508
509
510
511
512
513
514
515
516
517
518

Fig. 1 Maps showing location and geology of the Totalp area. **a** Location of the Totalp area in the tectonic map of the Alps (from Schmid et al. 2004; modified by Mohn et al. 2010). **b** Location of Totalp as a part of the South Penninic units in Grisons (Manatschal et al. 2003). **c** Geological map of Totalp (modified from Picazo et al. 2013) showing location of the analysed samples as well as the distribution of the major lithologies and samples described in this study (for description of samples see Table 1).

501
502
503
504
505
506
507
508
509
510
511
512
513
514
515
516
517
518

Fig. 2 Sketch showing the lithologies and the stratigraphy of the Totalp area (Weissert and Bernoulli 1985; Früh-Green et al. 1990; Manatschal et al. 2003; Picazo et al. 2013).

501
502
503
504
505
506
507
508
509
510
511
512
513
514
515
516
517
518

Fig. 3 The sulphide bearing outcrop in the Totalp area showing weathered lithology. Red circles are the sampling location in this outcrop. In the line-drawing on the right, light red identifies radiolarian cherts, dark red siliceous shale and yellow sulphate rich carbonate, rich in silica. **A** Zoom of outcrop. **b** Sample 65 is composed by calcite 50%. 25% quartz and is highly weathered. **c** Sample shows visible hematite crystals and calcite as the major mineral. **d** Sample 60 shows a siliceous rock with 3 different colours composed by 83% quartz , 10% albite and pyrite, illite and chlorite.

501
502
503
504
505
506
507
508
509
510
511
512
513
514
515
516
517
518

Fig. 4 **a** Global range of carbon isotopic composition of carbonates precipitated during early diagenetic processes (modified after Coleman et al. 1993; Kiriakoulakis 1996; Heydari 1997). **b** Carbon and oxygen isotopic composition of calcite veins in Totalp samples. **c** Limestone (sample 19) showing two generation of calcite veins.

519 Fig. 5 Representative mass chromatograms of the HCs of a typical sample of limestone
1
2 (sample 10) and a siliceous rock from the sulphide rich outcrop of Totalp (sample 60). **a** *n*-
3 alkanes (*m/z* 85) of sample 10 (limestone) **b** sterane distribution (*m/z* 217, 218) of sample
4
5 60 **c** PAH distribution (*m/z* 178, 192, 202, 228) of sample 60. For abbreviations see
7
8 appendix
9
10

11
12 524
13
14 525 Fig. 6 Thermal maturity parameters of C₂₇ steranes for Totalp samples. The classification
15 is from Peters *et al.*, 2005. The brown shaded area represents the range of complete
16
17 isomerization for the 20S/(20S + 20R) aaa C₂₇ steranes (*ca.* 55%) and αββ/(ααα + αββ) C₂₇
18
19 steranes (*ca.* 68%).
20
21
22

23
24 529
25
26 530 Fig. 7 Plot of pristane/n-C₁₇ vs phytane/n-C₁₈ for Totalp samples used to identify
27 depositional environment and OM type (after Peters *et al.* 1999).
28
29

30
31 532
32
33
34 533 Fig. 8 Sterane ternary distribution of the analysed samples for the αββ steranes of Totalp
35
36 534 samples. The interpretation of depositional environment is from Patrycja Wójcik-Tabol &
37
38
39 535 Ślączka (2015).
40
41

42
43
44 537 Fig. 9 Conceptual model explaining origin and migration of OM from the seawater into
45 different lithologies in the Totalp unit. **a** The OM is represented by particulate and dissolved
46 538 organic matter (POM and DOM, respectively). The OM infiltrates the basement rock by
47
48 539 rock-fluid circulation. **b** Some OM may be deposited within the carbonate veins (*e.g.* calcite
49
50 540 veins). **c** OM circulates with fluids through fractures and porosity of sediments to migrate
51
52 541 into the basement rock. **d** OM is preserved at the surfaces and in the interlayer surfaces of
53
54 clay minerals in the sediments.
55
56
57
58
59
60
61
62
63
64
65

544
1
545 Table 1. Results by lithology including mineralogy and texture observed in hand specimens
2
546 and the texture on the calcites used for the isotopic analyses ($\delta^{13}\text{C}_{\text{VPDB}}$, $\delta^{18}\text{O}_{\text{VPDB}}$). The vein
3
547 generation is defined from the specific example and may not correlate across all samples.¹
4
548 Thin section of the lithology is observed. • All lithology are from the lower sub-unit with
5
549 the exception of the massive serpentinite (samples 77, 78).
6
550
7
551

14
550
15
551 Table 2. Results by lithology including TC, TOC and total HC concentration in ppm (parts
16
552 per million) and organic carbon isotopic composition of bulk rock $\delta^{13}\text{C}_{\text{organic}}$. For the *n*-
17
553 alkanes: the carbon number range (*n*-alkane range), the maximum carbon number (Cmax),
18
554 carbon preference index (CPI values) and mean carbon number (MC#) are shown. For the
19
555 steranes, hopanes and PAHs the concentrations are in ppm and are represented in intervals
20
556 by star symbol *, where * = [0 - 0.1], ** = [0.1 - 1) and *** = [1 - 10) and BDL = below
21
557 detection limit. a: identified PAHs in the samples were: Phenanthrene, P; Fluoranthene,
22
558 Fluo; Pyrene, Pyr; Chrysene, Chry; Benzo(a)anthracene, BaA; Benzo(b)fluoranthene,
23
559 BbF; Benzo(a)pyrene, BaP; Indeno(1,2,3-cd)pyrene, IndPy; Benzo(ghi)perylene, BghiP;
24
560 Dibenzothiophene (DBT) , methylP (3,2,1 and 9 MPs) and 2-methyl naphthalene ; not all
25
561 were present in every sample. 1 All lithology are from lower sub-unit except the massive
26
562 serpentinite (samples 77, 78) which is from upper sub-unit
27
563
28
564

29
563 **References**
30
564
31
565 Arshad, A., Speth, D. R., de Graaf, R. M., den Camp, H. J. O., Jetten, M. S., Welte, C. U.
32
566 (2015). A metagenomics-based metabolic model of nitrate-dependent anaerobic
33
567 oxidation of methane by Methanoperedens-like archaea. *Frontiers in microbiology*, 6.
34
568
35
569
36
570
37
571
38
572
39
573
40
574
41
575
42
576
43
577
44
578
45
579
46
580
47
581
48
582
49
583
50
584
51
585
52
586
53
587
54
588
55
589
56
590
57
591
58
592
59
593
60
594
61
595
62
596
63
597
64
598
65

- 568 Bailey, S. W. (1969). Polytypism of trioctahedral 1: 1 layer silicates. *Clays and Clay
1 Minerals*, 17, 355-371.
2
3
4
5 Beard, J. S., & Hopkinson, L. (2000). A fossil, serpentinization-related hydrothermal vent,
6
7 Ocean Drilling Program Leg 173, Site 1068 (Iberia Abyssal Plain): Some aspects of
8 mineral and fluid chemistry. *Journal of Geophysical Research: Solid Earth* (1978–
9 10 11 12 13 14 15 16 17 18 19 20 21 22 23 24 25 26 27 28 29 30 31 32 33 34 35 36 37 38 39 40 41 42 43 44 45 46 47 48 49 50 51 52 53 54 55 56 57 58 59 60 61 62 63 64 65 2012), 105, 16527-16539.
14 574 Berner, R. A. (1984). Sedimentary pyrite formation: An update. *Geochimica et
15 Cosmochimica Acta*, 48, 605-615.
16
17 575 Bernoulli, D., & Weissert, H. (1985). Sedimentary fabrics in Alpine ophicalcites, south
18 Pennine Arosa zone, Switzerland. *Geology*, 13, 755-758.
19
20 576 Bernoulli, D., Manatschal, G., Desmurs, L., Muntener, O. (2003). Where did Gustav
21 Steinmann see the trinity? Back to the roots of an Alpine ophiolite concept. *Special
22 papers - geological society of America*, 373, 93-110.
23
24 578 Bernoulli, D., & Jenkyns, H. C. (2009). Ophiolites in ocean–continent transitions: from the
25 Steinmann Trinity to sea-floor spreading. *Comptes Rendus Geoscience*, 341, 363-381.
26
27 581 Blumenberg, M., Seifert, R., Reitner, J., Pape, T., Michaelis, W. (2004). Membrane lipid
28 patterns typify distinct anaerobic methanotrophic consortia. *Proceedings of the
29 National Academy of Sciences of the United States of America*, 101, 11111-11116.
30
31 582 Bougault, H., Charlou, J. L., Fouquet, Y., Needham, H. D., Vaslet, N., Appriou, P., Baptiste,
32 P. J., Rona, P. A., Dmitriev, L., Silantiev, S. (1993). Fast and slow spreading ridges:
33 structure and hydrothermal activity, ultramafic topographic highs, and CH₄ output.
34
35 583 Journal of Geophysical Research: Solid Earth, 98, 9643-9651.
36
37 584 Bradley, A. S., & Summons, R. E. (2010). Multiple origins of methane at the Lost City
38 Hydrothermal Field. *Earth and Planetary Science Letters*, 297, 34-41.
39
40
41
42
43
44
45
46
47
48
49
50
51
52
53
54
55
56
57
58
59
60
61
62
63
64
65

- 592 Burkhard, D. J., & O'Neil, J. R. (1988). Contrasting serpentinization processes in the eastern
1
593 Central Alps. *Contributions to Mineralogy and Petrology*, 99, 498-506.
2
594 Cardace, D., Hoehler, T., McCollom, T., Schrenk, M., Carnevale, D., Kubo, M., Twing, K.
3
595 (2013). Establishment of the Coast Range ophiolite microbial observatory (CROMO):
4
drilling objectives and preliminary outcomes. *Scientific Drilling*, 16, 45-55.
5
596
10
597 Charlou, J. L., Dmitriev, L., Bougault, H., Needham, H. D. (1988). Hydrothermal CH4
11
between 12°N and 15°N over the Mid-Atlantic Ridge. *Deep Sea Research Part A.*
12
13
598 *Oceanographic Research Papers*, 35, 121-131.
14
15
599
16
600 Charlou, J. L., & Donval, J. P. (1993). Hydrothermal methane venting between 12°N and
17
26°N along the Mid-Atlantic Ridge. *Journal of Geophysical Research*, 98, 9625-
18
9642.
19
20
601
21
22
602
23
24
603 Charlou, J. L., Fouquet, Y., Bougault, H., Donval, J. P., Etoubleau, J., Jean-Baptiste, P.,
25
26
27
604 Dapoigny, A., Appriou, P., Rona, P. A. (1998). Intense CH4 plumes generated by
28
serpentinization of ultramafic rocks at the intersection of the 15°20'N fracture zone
29
30
31
605 and the Mid-Atlantic Ridge. *Geochimica et Cosmochimica Acta*, 62, 2323-2333.
32
33
34
606
35
36
607 Charlou, J. L., Donval, J. P., Fouquet, Y., Jean-Baptiste, P., Holm, N. (2002). Geochemistry
37
of high H2 and CH4 vent fluids issuing from ultramafic rocks at the Rainbow
38
40
hydrothermal field (36°14'N, MAR). *Chemical Geology*, 191, 345-359.
41
42
609
43
610 Coleman, M., Raiswell, R., Brown, A., Curtis, C., Aplin, A., Ortoleva, P., Gruszczynski, M.,
44
45
611 Lyons, T., Lovley, D., Eglington, G. (1993). Microbial mineralization of organic
46
47
matter: mechanisms of self-organization and inferred rates of precipitation of
48
49
612 diagenetic minerals [and Discussion]. *Philosophical Transactions of the Royal
50
51
613 Society of London A: Mathematical, Physical and Engineering Sciences*, 344, 69-87.
52
53
614
54
55
56
57
58
59
60
61
62
63
64
65

- 615 Craig, H. (1957). Isotopic standards for carbon and oxygen and correction factors for mass-
1
616 spectrometric analysis of carbon dioxide. *Geochimica et Cosmochimica Acta*, 12,
2
617 133-149.
3
618 Delacour, A., Früh-Green, G. L., Bernasconi, S. M., Schaeffer, P., Kelley, D. S. (2008).
4
619 Carbon geochemistry of serpentinites in the Lost City Hydrothermal System (30°N,
5
620 MAR). *Geochimica et Cosmochimica Acta*, 72, 3681-3702.
7
621 Desmurs, L., Müntener, O., Manatschal, G. (2002). Onset of magmatic accretion within a
8
622 magma-poor rifted margin: a case study from the Platta ocean-continent transition,
9
623 eastern Switzerland. *Contributions to Mineralogy and Petrology*, 144, 365-382.
10
624 Dias, Á. S., & Barriga, F. J. (2006). Mineralogy and geochemistry of hydrothermal sediments
11
625 from the serpentinite-hosted Saldanha hydrothermal field (36 34' N; 33 26' W) at
12
626 MAR. *Marine geology*, 225, 157-175.
13
627 Dix, G. R., & Mullins, H. T. (1992). Shallow-burial diagenesis of deep-water carbonates,
14
628 northern Bahamas: Results from deep-ocean drilling transects. *Geological Society of
15
629 America Bulletin*, 104, 303-315.
16
630 Etiope, G., & Ionescu, A. (2014). Low-temperature catalytic CO₂ hydrogenation with
17
631 geological quantities of ruthenium: a possible abiotic CH₄ source in chromitite-rich
18
632 serpentinized rocks. *Geofluids*, 5, 438-452.
19
633 Fabiańska, M., Kozielska, B., Bielaczyc, P., Woodburn, J., Konieczyński, J. (2016).
20
634 Geochemical markers and polycyclic aromatic hydrocarbons in solvent extracts from
21
635 diesel engine particulate matter. *Environmental Science and Pollution Research*, 23,
22
636 6999-7011.
23
637 Farough, A., Moore, D., Lockner, D., Lowell, R. (2016). Evolution of fracture permeability
24
638 of ultramafic rocks undergoing serpentinization at hydrothermal conditions: An
25
639 experimental study. *Geochemistry, Geophysics, Geosystems*, 17, 44-55.

- 1 640 Frazer, J. W., & Crawford, R. (1963). Modifications in the simultaneous determination of
2 641 carbon, hydrogen, and nitrogen. *Microchimica Acta*, 51, 561-566.
3
4 642 Friedman, I., & O'Neil, J. R., (1977), Data of geochemistry: Compilation of stable isotope
5 fractionation factors of geochemical interest pp.). US Government Printing Office.
6
7 643 Früh-Green, G. L., Weissert, H., Bernoulli, D. (1990). A multiple fluid history recorded in
8 Alpine ophiolites. *Journal of the Geological Society*, 147, 959-970.
9
10 644 Geissman, T., Sim, K., Murdoch, J. (1967). Organic minerals. Picene and chrysene as
11 constituents of the mineral curtisite (idrialite). *Cellular and Molecular Life Sciences*,
12 645 23, 793-794.
13
14 646 Gonçalves, P. A., Mendonça Filho, J. G., Mendonça, J. O., da Silva, T. F., Flores, D. (2013).
15
16 647 Paleoenvironmental characterization of a Jurassic sequence on the Bombarral sub-
17 648 basin (Lusitanian basin, Portugal): insights from palynofacies and organic
18 geochemistry. *International Journal of Coal Geology*, 113, 27-40.
19
20 649 Gràcia, E., Charlou, J. L., Radford-Knoery, J., Parson, L. M. (2000). Non-transform offsets
21 along the Mid-Atlantic Ridge south of the Azores (38 N–34 N): ultramafic exposures
22
23 650 and hosting of hydrothermal vents. *Earth and Planetary Science Letters*, 177, 89-103.
24
25 651 652 Grantham, P. J., & Wakefield, L. L. (1988). Variations in the sterane carbon number
26 distributions of marine source rock derived crude oils through geological time.
27
28 653 654 655 656 657 658 659 660 661 662 663 664
29 655 656 657 658 659 660 661 662 663 664
30 655 656 657 658 659 660 661 662 663 664
31 655 656 657 658 659 660 661 662 663 664
32 655 656 657 658 659 660 661 662 663 664
33 655 656 657 658 659 660 661 662 663 664
34 655 656 657 658 659 660 661 662 663 664
35 655 656 657 658 659 660 661 662 663 664
36 655 656 657 658 659 660 661 662 663 664
37 655 656 657 658 659 660 661 662 663 664
38 655 656 657 658 659 660 661 662 663 664
39 655 656 657 658 659 660 661 662 663 664
40 655 656 657 658 659 660 661 662 663 664
41 655 656 657 658 659 660 661 662 663 664
42 655 656 657 658 659 660 661 662 663 664
43 655 656 657 658 659 660 661 662 663 664
44 655 656 657 658 659 660 661 662 663 664
45 655 656 657 658 659 660 661 662 663 664
46 655 656 657 658 659 660 661 662 663 664
47 655 656 657 658 659 660 661 662 663 664
48 655 656 657 658 659 660 661 662 663 664
49 655 656 657 658 659 660 661 662 663 664
50 655 656 657 658 659 660 661 662 663 664
51 655 656 657 658 659 660 661 662 663 664
52 655 656 657 658 659 660 661 662 663 664
53 655 656 657 658 659 660 661 662 663 664
54 655 656 657 658 659 660 661 662 663 664
55 655 656 657 658 659 660 661 662 663 664
56 655 656 657 658 659 660 661 662 663 664
57 655 656 657 658 659 660 661 662 663 664
58 655 656 657 658 659 660 661 662 663 664
59 655 656 657 658 659 660 661 662 663 664
60 655 656 657 658 659 660 661 662 663 664
61 655 656 657 658 659 660 661 662 663 664
62 655 656 657 658 659 660 661 662 663 664
63 655 656 657 658 659 660 661 662 663 664
64 655 656 657 658 659 660 661 662 663 664
65 655 656 657 658 659 660 661 662 663 664

- 1 Hayes, J. M., Freeman, K. H., Popp, B. N., Hoham, C. H. (1990). Compound-specific
2 isotopic analyses: A novel tool for reconstruction of ancient biogeochemical
3 processes. *Organic geochemistry*, 16, 1115-1128.
4
5
6
7 Haymon, R. M. (1983). Hydrothermal deposition on the East Pacific Rise at 21 N. *Journal of*
8
9 *Geochemical Exploration*, 19, 493-495.
10
11
12 Haymon, R. M. (1989). Hydrothermal processes and products on the Galapagos Rift and East
13
14 Pacific Rise. In D.M. Hussong E.L. Winterer, & R.W. Decker (ed.), *The Eastern*
15
16 *Pacific Ocean and Hawaii*, (pp.125-144): Geological Society of America.
17
18
19 Heydari, E. (1997). Hydrotectonic models of burial diagenesis in platform carbonates based
20
21 on formation water geochemistry in North American sedimentary basins. In I.P.
22
23 Montanez, J.M. Gregg&K.L.Shelton (ed.), *Basin-wide diagenetic patterns:Integrated*
24
25 *petrologic, geochemical and hydrologic considerations*, (pp.53-79): Society of
26
27 Economic Paleontologists and Mineralogists, Special Publication
28
29
30 Heymann, D., Jenneskens, L. W., Jehlicka, J., Koper, C., Vlietstra, E. J. (2003). Biogenic
31
32 fullerenes? *International Journal of Astrobiology*, 2, 179-183.
33
34
35 Hinrichs, K.-U., Summons, R. E., Orphan, V., Sylva, S. P., Hayes, J. M. (2000). Molecular
36
37 and isotopic analysis of anaerobic methane-oxidizing communities in marine
38
39 sediments. *Organic geochemistry*, 31, 1685-1701.
40
41
42 Holm, N. G., Dumont, M., Ivarsson, M., Konn, C. (2006). Alkaline fluid circulation in
43
44 ultramafic rocks and formation of nucleotide constituents: a hypothesis. *Geochemical*
45
46 *Transactions*, 7, 1-13.
47
48
49 Hudson, J. (1977). Stable isotopes and limestone lithification. *Journal of the Geological*
50
51 *Society*, 133, 637-660.
52
53
54 Jamtveit, B., & Hammer, Ø. (2012). Sculpting of rocks by reactive fluids. *Geochemical*
55
56 *Perspectives*, 1, 341-342.
57
58
59
60
61
62
63
64
65

- 690 Kawka, O. E., & Simoneit, B. R. (1990). Polycyclic aromatic hydrocarbons in hydrothermal
1
691 petroleums from the Guaymas Basin spreading center. *Applied Geochemistry*, 5, 17-
2
692 27.
3
693 Kelley, D. S., & Delaney, J. R. (1987). Two-phase separation and fracturing in mid-ocean
4
694 ridge gabbros at temperatures greater than 700 C. *Earth and Planetary Science
5*
Letters, 83, 53-66.
6
695
7 Kelley, D. S., Karson, J. A., Blackman, D. K., Fruh-Green, G. L., Butterfield, D. A., Lilley,
8
696 M. D., Olson, E. J., Schrenk, M. O., Roe, K. K., Lebon, G. T., Rivizzigno, P., the, A.
9
697 T. S. P. (2001). An off-axis hydrothermal vent field near the Mid-Atlantic Ridge at
10
698 30[deg] N. *Nature*, 412, 145-149.
11
699
12 Kelley, D. S., Karson, J. A., Früh-Green, G. L., Yoerger, D. R., Shank, T. M., Butterfield, D.
13
700 A., Hayes, J. M., Schrenk, M. O., Olson, E. J., Proskurowski, G. (2005). A
14
701 serpentinite-hosted ecosystem: the Lost City hydrothermal field. *Science*, 307, 1428-
15
702 1434.
16
703
17 Kelley, D. S., & Shank, T. M. (2010). Hydrothermal systems: A decade of discovery in slow
18
704 spreading environments. In C. W. Devey P. A. Rona, J. Dyment and B. J. Murton
19
705 (ed.), *Diversity of Hydrothermal Systems on Slow Spreading Ocean Ridges*, (pp.369-
20
706 407) Washington: American Geophysical Union.
21
707
22 Kennedy, M. J., Pevear, D. R., Hill, R. J. (2002). Mineral surface control of organic carbon in
23
708 black shale. *Science*, 295, 657-660.
24
709
25 Killops, S., & Massoud, M. (1992). Polycyclic aromatic hydrocarbons of pyrolytic origin in
26
710 ancient sediments: evidence for Jurassic vegetation fires. *Organic geochemistry*, 18,
27
711 1-7.
28
712
29
55
56
57
58
59
60
61
62
63
64
65

- 713 Lemoine, M., Tricart, P., Boillot, G. (1987). Ultramafic and gabbroic ocean floor of the
1
2 Ligurian Tethys (Alps, Corsica, Apennines): In search of a genetic imodel. *Geology*,
3
4 715 15, 622-625.
5
6
7 716 Mackenzie, A., Patience, R., Maxwell, J., Vandenbroucke, M., Durand, B. (1980). Molecular
8
9 parameters of maturation in the Toarcian shales, Paris Basin, France—I. Changes in
10
11 the configurations of acyclic isoprenoid alkanes, steranes and triterpanes. *Geochimica*
12
13 718 *et Cosmochimica Acta*, 44, 1709-1721.
14
15
16 720 Manatschal, G., & Bernoulli, D. (1999). Architecture and tectonic evolution of nonvolcanic
17
18 margins: Present-day Galicia and ancient Adria. *Tectonics*, 18, 1099-1119.
19
20
21 722 Manatschal, G., Froitzheim, N., Rubenach, M., Turrin, B. D. (2001). The role of detachment
22
23 faulting in the formation of an ocean-continent transition: insights from the Iberia
24
25 723 Abyssal Plain. *Geological Society, London, Special Publications*, 187, 405-428.
26
27
28 725 Manatschal, G., Muntener, O., Desmurs, L., Bernoulli, D. (2003). An ancient ocean-continent
29
30 transition in the Alps: the Totalp, Err-Platta, and Malenco units in the eastern Central
31
32 726 Alps (Graubünden and northern Italy). *Eclogae Geologicae Helvetiae*, 96, 131-146.
33
34
35 728 McCollom, T. M., & Shock, E. L. (1997). Geochemical constraints on chemolithoautotrophic
36
37 metabolism by microorganisms in seafloor hydrothermal systems. *Geochimica et*
38
39 729 *Cosmochimica Acta*, 61, 4375-4391.
40
41
42 731 McCollom, T. M. (2013). Laboratory simulations of abiotic hydrocarbon formation in Earth's
43
44 deep subsurface. *Reviews in Mineralogy & Geochemistry*, 75, 467-494.
45
46
47 732 McCollom, T. M., & Seewald, J. S. (2013). Serpentinites, Hydrogen, and Life. *Elements*, 9,
48
49 733 129-134.
50
51
52 735 McCollom, T. M., & Donaldson, C. (2016). Generation of Hydrogen and Methane during
53
54 Experimental Low-Temperature Reaction of Ultramafic Rocks with Water.
55
56 736
57
58 737 *Astrobiology*, 16, 389-406.
59
60
61
62
63
64
65

- 1 738 McCrea, J. M. (1950). On the isotopic chemistry of carbonates and a paleotemperature scale.
- 2 739 *The Journal of Chemical Physics*, 18, 849-857.
- 3
- 4 740 Ménez, B., Pasini, V., Brunelli, D. (2012). Life in the hydrated suboceanic mantle. *Nature*
- 5
- 6 741 *Geoscience*, 5, 133-137.
- 7
- 8
- 9 742 Mohn, G., Manatschal, G., Müntener, O., Beltrando, M., Masini, E. (2010). Unravelling the
- 10
- 11 743 interaction between tectonic and sedimentary processes during lithospheric thinning in
- 12
- 13 744 the Alpine Tethys margins. *International Journal of Earth Sciences*, 99, 75-101.
- 14
- 15
- 16 745 Montgomery, H., & Kerr, A. C. (2009). Rethinking the origins of the red chert at La Désirade,
- 17
- 18 746 French West Indies. *Geological Society, London, Special Publications*, 328, 457-467.
- 19
- 20 747 Mottl, M. J., Komor, S. C., Fryer, P., Moyer, C. L. (2003). Deep-slab fluids fuel
- 21
- 22 748 extremophilic Archaea on a Mariana forearc serpentinite mud volcano: Ocean Drilling
- 23
- 24 749 Program Leg 195. *Geochemistry, Geophysics, Geosystems*, 4, 1525-2027.
- 25
- 26
- 27 750 Müntener, O., Pettke, T., Desmurs, L., Meier, M., Schaltegger, U. (2004). Refertilization of
- 28
- 29 751 mantle peridotite in embryonic ocean basins: trace element and Nd isotopic evidence
- 30
- 31 752 and implications for crust–mantle relationships. *Earth and Planetary Science Letters*,
- 32
- 33 753 221, 293-308.
- 34
- 35
- 36 754 Müntener, O., Manatschal, G., Desmurs, L., Pettke, T. (2010). Plagioclase peridotites in
- 37
- 38 755 ocean–continent transitions: refertilized mantle domains generated by melt stagnation
- 39
- 40 756 in the shallow mantle lithosphere. *Journal of Petrology*, 51, 255-294.
- 41
- 42
- 43 757 Orem, W. H., Spiker, E. C., Kotra, R. K. (1990). Organic matter in hydrothermal metal ores
- 44
- 45 758 and hydrothermal fluids. *Applied Geochemistry*, 5, 125-134.
- 46
- 47
- 48 759 Orphan, V. J., House, C. H., Hinrichs, K.-U., McKeegan, K. D., DeLong, E. F. (2001).
- 49
- 50
- 51 760 Methane-consuming archaea revealed by directly coupled isotopic and phylogenetic
- 52
- 53 761 analysis. *Science*, 293, 484-487.
- 54
- 55
- 56
- 57
- 58
- 59
- 60
- 61
- 62
- 63
- 64
- 65

- 762 Peltzer, E., & Gagosian, R. (1989). Organic geochemistry of aerosols over the Pacific Ocean.
1
2 763 *Chemical oceanography*, 10, 281-338.
3
4 764 Peters, K., Walters, C., Moldowan, J., (2005a), The Biomarker Guide: 2, Biomarkers and
5 Isotopes in Petroleum Systems and Earth History. (700 pp.). Cambridge University
6
7 765 Press.
8
9 766
10
11
12 767 Peters, K. E., Fraser, T. H., Amris, W., Rustanto, B., Hermanto, E. (1999). Geochemistry of
13 crude oils from eastern Indonesia. *The American Association of Petroleum Geologists*
14
15 768 83, 1927-1942.
16
17 769
18
19 770 Peters, K. E., Walters, C. C., Moldowan, J. M., (2005b), The biomarker guide: 1, Biomarkers
20 and isotopes in the environment and human history (490 pp.). Cambridge University
21
22 771 Press.
23
24 772
25
26
27 773 Peters, T. (1968). Distribution of Mg, Fe, Al, Ca and Na in Coexisting Olivine,
28
29 774 Orthopyroxene and Clinopyroxene in the Totalp Serpentinite (Davos, Switzerland)
30
31 775 and in the Alpine Metamorphosed Malenco Serpentinite (N. Italy). *Contributions to*
32
33 776 *Mineralogy and Petrology*, 18, 65-75.
34
35
36 777 Peters, T., & Stettler, A. (1987). Radiometric age, thermobarometry and mode of
37 emplacement of the Totalp peridotite in the Eastern Swiss Alps. . *Schweizerische*
38
39 778 *Mineralogische und Petrographische Mitteilungen*, 67, 285-294.
40
41 779
42
43 780 Picazo, S., Manatschal, G., Cannat, M., Andréani, M. (2013). Deformation associated to
44 exhumation of serpentинized mantle rocks in a fossil Ocean Continent Transition: The
45
46 781 Totalp unit in SE Switzerland. *Lithos*, 175-176, 255-271.
47
48 782
49
50
51 783 Proskurowski, G., Lilley, M. D., Seewald, J. S., Früh-Green, G. L., Olson, E. J., Lupton, J. E.,
52
53 784 Sylva, S. P., Kelley, D. S. (2008). Abiogenic hydrocarbon production at Lost City
54
55 785 hydrothermal field. *Science*, 319, 604-607.
56
57
58
59
60
61
62
63
64
65

- 1 786 Raghoebarsing, A. A., Pol, A., Van de Pas-Schoonen, K. T., Smolders, A. J., Ettwig, K. F.,
2 787 Rijpstra, W. I. C., Schouten, S., Damsté, J. S. S., den Camp, H. J. O., Jetten, M. S.
3
4 788 (2006). A microbial consortium couples anaerobic methane oxidation to
5
6
7 789 denitrification. *Nature*, 440, 918-921.
8
9 790 Reeves, E. P., McDermott, J. M., Seewald, J. S. (2014). The origin of methanethiol in
10
11 791 midocean ridge hydrothermal fluids. *Proceedings of the National Academy of*
12
13 792 *Sciences of the United States of America*, 111, 5474-5479.
14
15
16 793 Rona, P., Widenfalk, L., Boström, K. (1987). Serpentized ultramafics and hydrothermal
17
18 794 activity at the Mid-Atlantic Ridge crest near 15 N. *Journal of Geophysical Research:*
19
20 795 *Solid Earth*, 92, 1417-1427.
21
22
23
24 796 Rona, P., Bougault, H., Charlou, J., Appriou, P., Nelsen, T., Trefry, J., Eberhart, G., Barone,
25
26
27 797 A., Needham, H. (1992). Hydrothermal circulation, serpentinization, and degassing at
28
29 798 a rift valley-fracture zone intersection: Mid-Atlantic Ridge near 15 N, 45 W. *Geology*,
30
31 799 20, 783-786.
32
33
34 800 Rona, P. A. (1984). Hydrothermal mineralization at seafloor spreading centers. *Earth-Science*
35
36 801 *Reviews*, 20, 1-104.
37
38
39 802 Saha, M., Togo, A., Mizukawa, K., Murakami, M., Takada, H., Zakaria, M. P., Chiem, N. H.,
40
41 803 Tuyen, B. C., Prudente, M., Boonyatumonond, R. (2009). Sources of sedimentary
42
43 804 PAHs in tropical Asian waters: differentiation between pyrogenic and petrogenic
44
45 805 sources by alkyl homolog abundance. *Marine pollution bulletin*, 58, 189-200.
46
47
48 806 Schidlowski, M. (1988). A 3,800-million-year isotopic record of life from carbon in
49
50
51 807 sedimentary rocks. *Nature*, 333, 313-318.
52
53
54 808 Schidlowski, M. (2001). Carbon isotopes as biogeochemical recorders of life over 3.8 Ga of
55
56 809 Earth history: evolution of a concept. *Precambrian Research*, 106, 117-134.
57
58
59
60
61
62
63
64
65

- 810 Seifert, W. K., & Moldowan, J. M. (1980). The effect of thermal stress on source-rock quality
1
2 as measured by hopane stereochemistry. *Physics and Chemistry of the Earth*, 12, 229-
3
4 237.
5
6
7 Shock, E. L., McCollom, T., Schulte, M. D. (2002). The emergence of metabolism from
8
9 within hydrothermal systems. In Juergen Wiegeland Adams W.W. Michael (ed.),
10
11 *Thermophiles: the keys to molecular evolution and the origin of life*, (pp.59-76): CRC
12
13 Press.
14
15
16
17 Simoneit, B., & Philp, R. (1982). Organic geochemistry of lipids and kerogen and the effects
18
19 of basalt intrusions in unconsolidated oceanic sediments site 477, site 478 and site
20
21 481, Guaymas basin, Gulf of California. In J.R. Curran & D.G. Moore (ed.), *Initial*
22
23 *Reports of the Deep Sea Drilling Project*, (pp.883-904) Washington: U.S.
24
25 Gouvernment Printing office.
26
27
28
29 Simoneit, B. R., Brenner, S., Peters, K., Kaplan, I. (1978). Thermal alteration of Cretaceous
30
31 black shale by basaltic intrusions in the Eastern Atlantic. *Nature*, 273, 501-504.
32
33
34 Sofer, Z. (1980). Preparation of carbon dioxide for stable carbon isotope analysis of
35
36 petroleum fractions. *Analytical chemistry*, 52, 1389-1391.
37
38
39 Styrt, M., Brackmann, A., Holland, H., Clark, B., Pisutha-Arnond, V., Eldridge, C., Ohmoto,
40
41 H. (1981). The mineralogy and the isotopic composition of sulfur in hydrothermal
42
43 sulfide/sulfate deposits on the East Pacific Rise, 21 N latitude. *Earth and Planetary*
44
45 *Science Letters*, 53, 382-390.
46
47
48 Summons, R. E., Jahnke, L. L., Roksandic, Z. (1994). Carbon isotopic fractionation in lipids
49
50 from methanotrophic bacteria: relevance for interpretation of the geochemical record
51
52 of biomarkers. *Geochimica et Cosmochimica Acta*, 58, 2853-2863.
53
54
55 Swart, P. K., Burns, S., Leder, J. (1991). Fractionation of the stable isotopes of oxygen and
56
57 carbon in carbon dioxide during the reaction of calcite with phosphoric acid as a
58
59
60
61
62
63
64
65

835 function of temperature and technique. *Chemical Geology: Isotope Geoscience*
1
2 836 section, 86, 89-96.
3

4 837 Templeton, A. S., Chu, K.-H., Alvarez-Cohen, L., Conrad, M. E. (2006). Variable carbon
5
6 isotope fractionation expressed by aerobic CH₄-oxidizing bacteria. *Geochimica et*
7
8 838 *Cosmochimica Acta*, 70, 1739-1752.
9
10

11 840 van Acken, D., Becker, H., Walker, R. J., McDonough, W. F., Wombacher, F., Ash, R. D.,
12
13 841 Piccoli, P. M. (2010). Formation of pyroxenite layers in the Totalp ultramafic massif
14
15 (Swiss Alps) – Insights from highly siderophile elements and Os isotopes.
16
17 842 *Geochimica et Cosmochimica Acta*, 74, 661-683.
18
19 843

20
21 844 Villanueva, J., Grimalt, J. O., Cortijo, E., Vidal, L., Labeyriez, L. (1997). A biomarker
22
23 approach to the organic matter deposited in the North Atlantic during the last climatic
24
25 cycle. *Geochimica et Cosmochimica Acta*, 61, 4633-4646.
26
27

28
29 847 Weissert, H., McKenzie, J., Channell, J. (1985). Natural variations in the carbon cycle during
30
31 the Early Cretaceous. In E.T. Sundquist and W.S. Broecker (ed.), *The Carbon Cycle*
32
33 and Atmospheric CO₂: Natural Variations Archean to Present, (pp.531-545)
34
35 Washington D.C.: American Geophysical Union Geophysical Monograph.
36
37 850

38
39 851 Weissert , H. J., & Bernoulli, D. (1985). A transform margin in the Mesozoic Tethys:
40
41 evidence from the Swiss Alps. *Geologische Rundschau*, 74, 665-679.
42

43
44 853 Williams, L. A., Parks, G. A., Crerar, D. A. (1985). Silica diagenesis, I. Solubility controls.
45
46 854 *Journal of Sedimentary Research*, 55, 301-311.
47

48
49 855 Wójcik-Tabol, P., & Ślączka, A. (2015). Are Early Cretaceous environmental changes
50
51 recorded in deposits of the Western part of the Silesian Nappe? A geochemical
52
53 approach. *Palaeogeography, Palaeoclimatology, Palaeoecology*, 417, 293-308.
54

55
56 858 Wolff, G. A., Boardman, D., Horsfall, I., Sutton, I., Davis, N., Chester, R., Ripley, M., Lewis,
57
58 859 C. A., Rowland, S. J., Patching, J. (1995). The biogeochemistry of sediments from the
59
60
61

- 860 Madeira Abyssal Plain—preliminary results. *Internationale Revue der gesamten*
1
2 861 *Hydrobiologie und Hydrographie*, 80, 333-349.
3
4 862 Zeng, Z., Niedermann, S., Chen, S., Wang, X., Li, Z. (2015). Noble gases in sulfide deposits
5
6 863 of modern deep-sea hydrothermal systems: Implications for heat fluxes and
7
8 864 hydrothermal fluid processes. *Chemical Geology*, 409, 1-11.
9
10
11
12 865
13
14
15
16
17
18
19
20
21
22
23
24
25
26
27
28
29
30
31
32
33
34
35
36
37
38
39
40
41
42
43
44
45
46
47
48
49
50
51
52
53
54
55
56
57
58
59
60
61
62
63
64
65

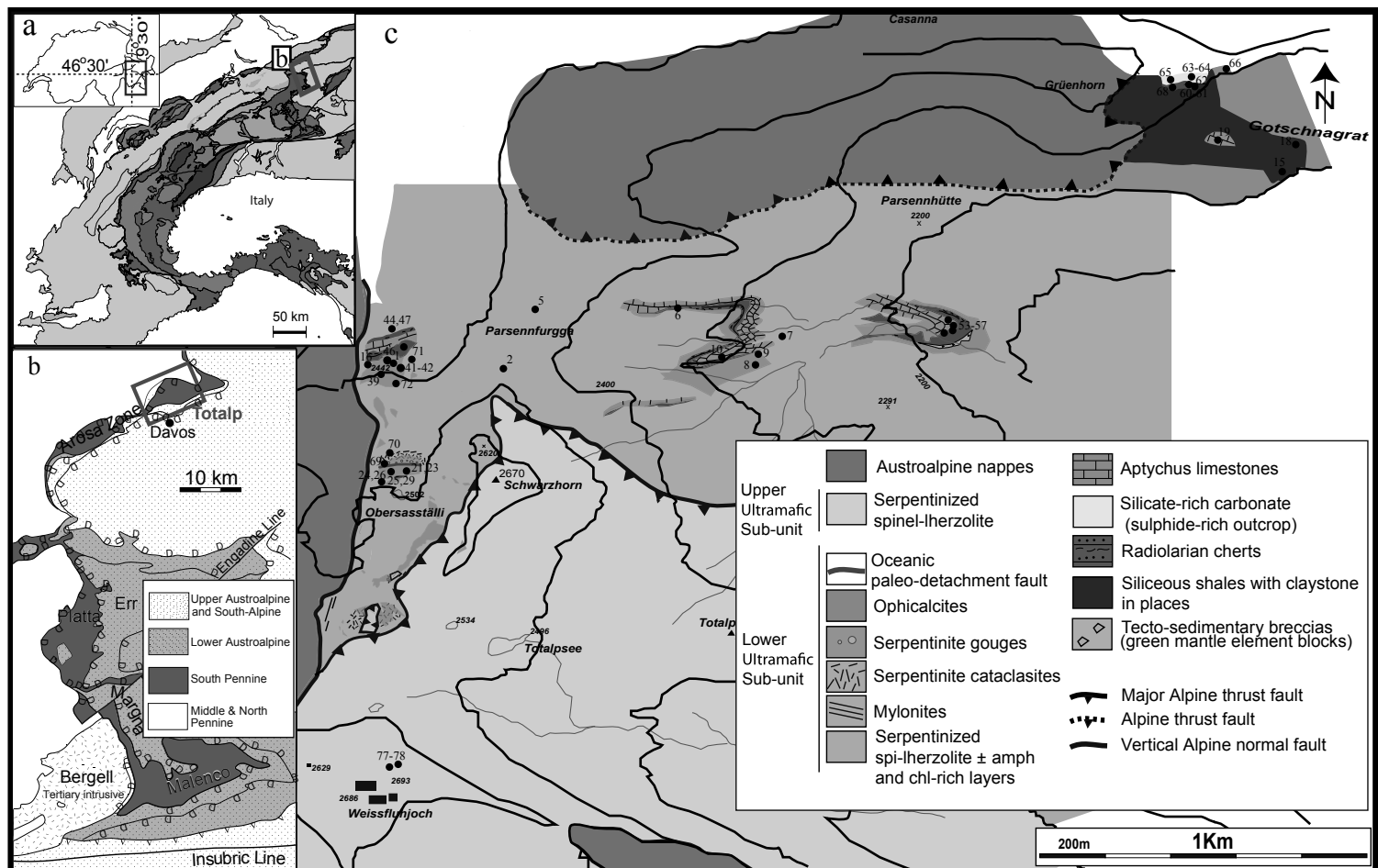


Fig 1. Maps showing location and geology of the Totalp area. **a** Location of the Totalp area in the tectonic map of the Alps (from Schmid *et al.* 2004, modified by Mohn *et al.* 2010). **b** Location of Totalp as a part of the South Pennine units in Grisons (Manatschal *et al.* 2003). **c** Geological map of Totalp (modified from Picazo *et al.* 2013) showing location of the analysed samples as well as the distribution of the major lithologies and samples described in this study (for description of samples see Table 1).

Log of Totalp exhumed mantle and sedimentary cover

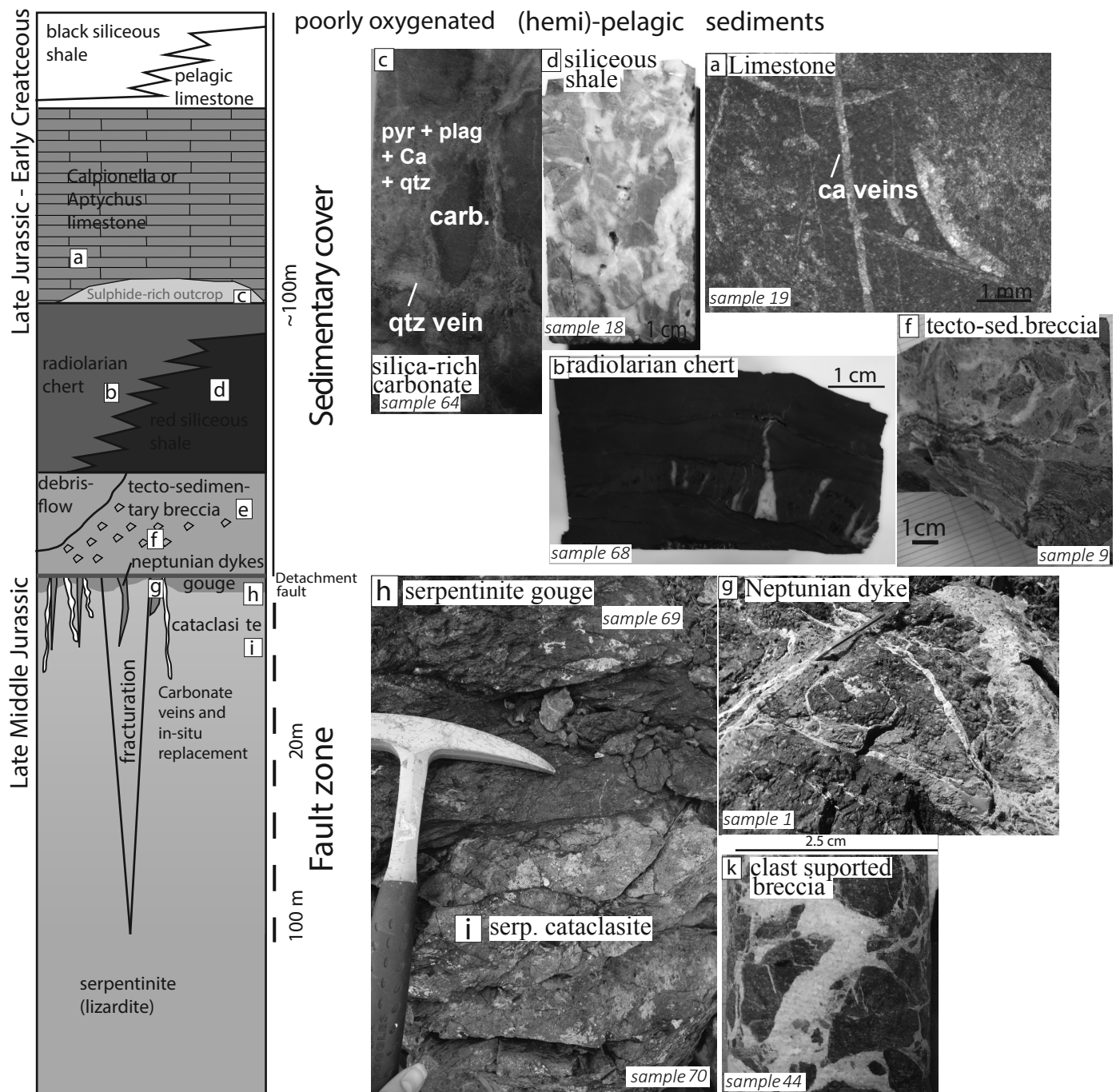


Fig. 2 Sketch showing the lithologies and the stratigraphy of the Totalp area (Weissert and Bernoulli 1985; Früh-Green et al. 1990; Manatschal et al. 2003; Picazo et al. 2013).

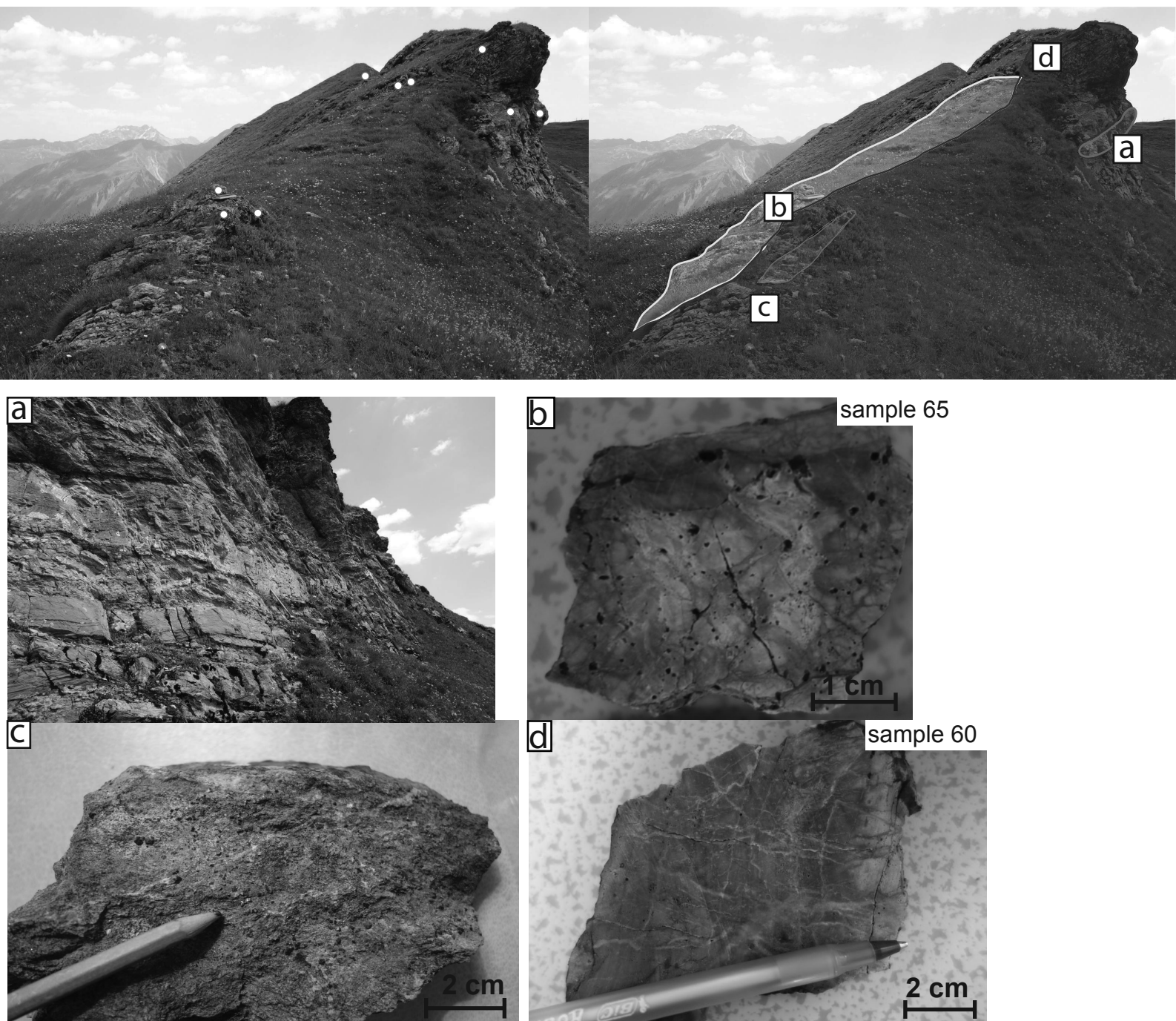


Fig 3. The sulphide bearing outcrop in the Totalp area showing weathered lithology. Circles show the sampling location for this outcrop. In the line-drawing on the right, light red identifies radiolarian cherts, dark red siliceous shale and yellow sulfite rich carbonate, rich in silica. **a** Zoom of outcrop. **b** Sample 65 is composed by calcite 50%, 25% quartz and is highly weathered. **c** Sample shows visible hematite crystals and calcite as the major mineral. **d** Sample 60 shows a siliceous rock with 3 different colours composed by 83% quartz , 10% albite and pyrite, illite and chlorite.

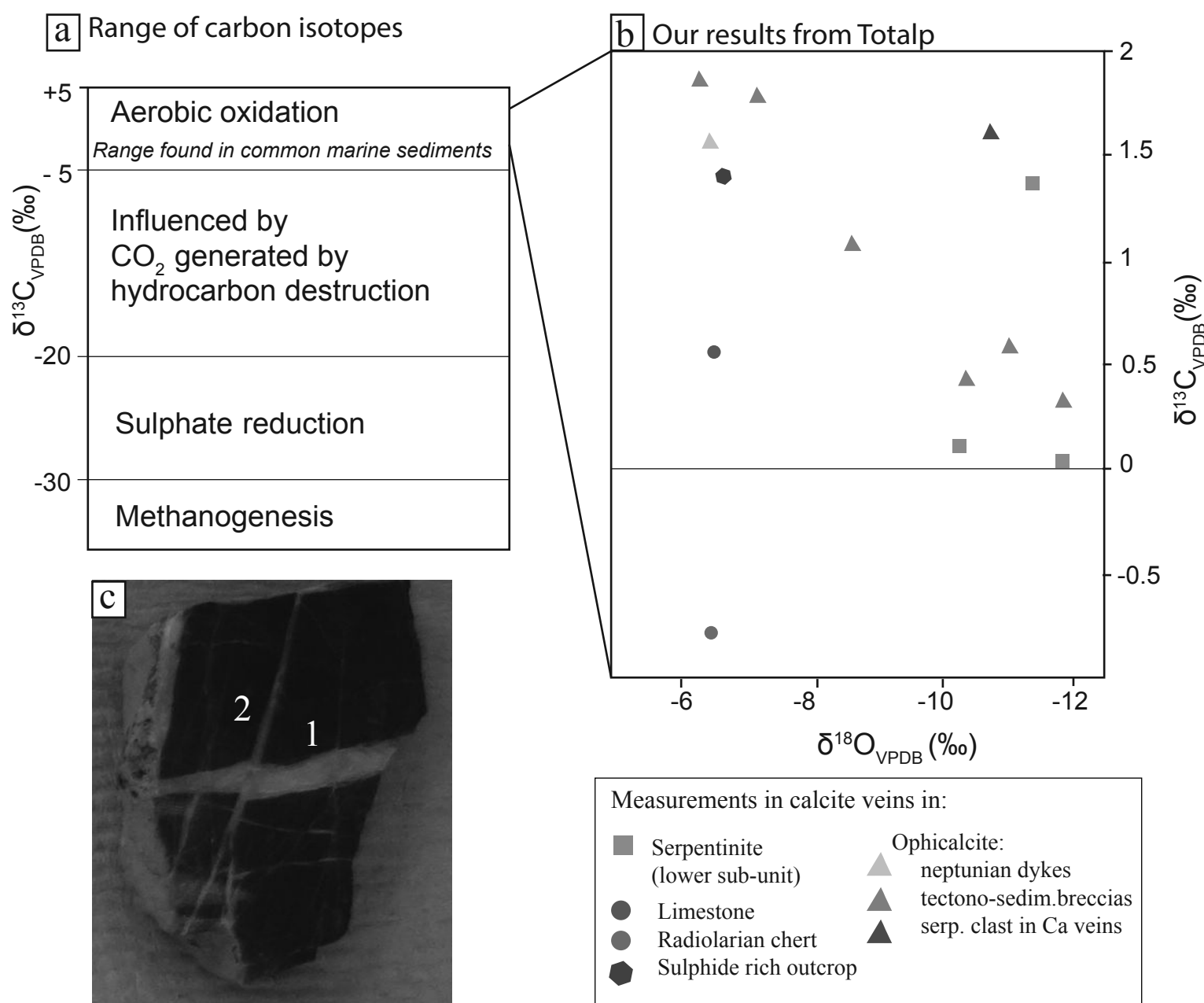


Fig. 4 **a** Global range of carbon isotopic composition of carbonates precipitated during early diagenetic processes (modified after Coleman *et al.* 1993; Kiriakoulakis 1996; Heydari 1997). **b** Carbon and oxygen isotopic composition of calcite veins in Totalp samples. **c** Limestone (sample 19) showing two generations of calcite veins.

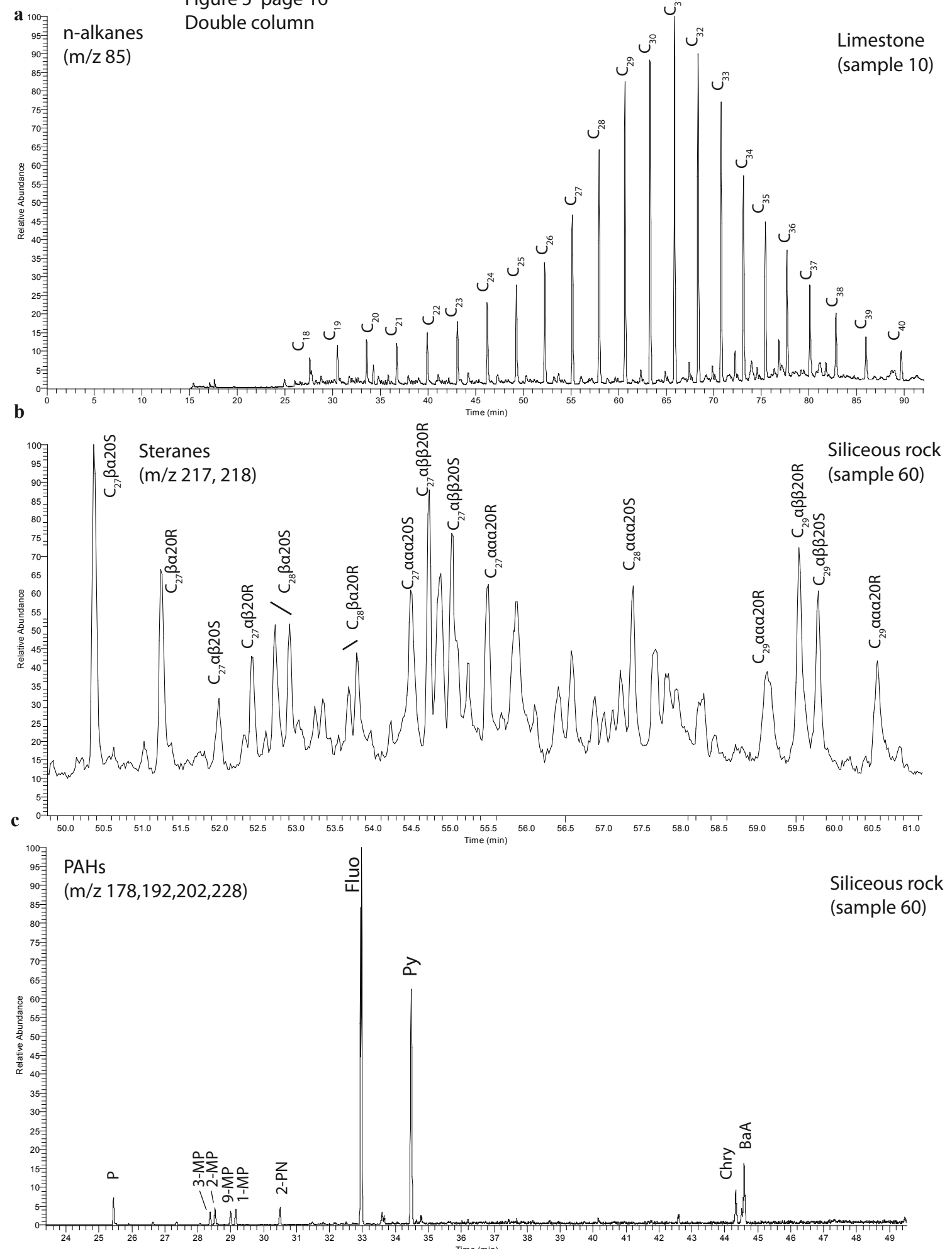


Fig. 5 Representative mass chromatograms of the HCs of a typical sample of limestone (sample 10) and a siliceous rock from the sulphide rich outcrop of Totalp (sample 60). **a** n-alkanes distribution (m/z 85) of sample 10 (limestone) **b** sterane distribution (m/z 217, 218) of sample 60 **c** PAH distribution (m/z 178, 192, 202, 228) of sample 60. For abbreviations see appendix

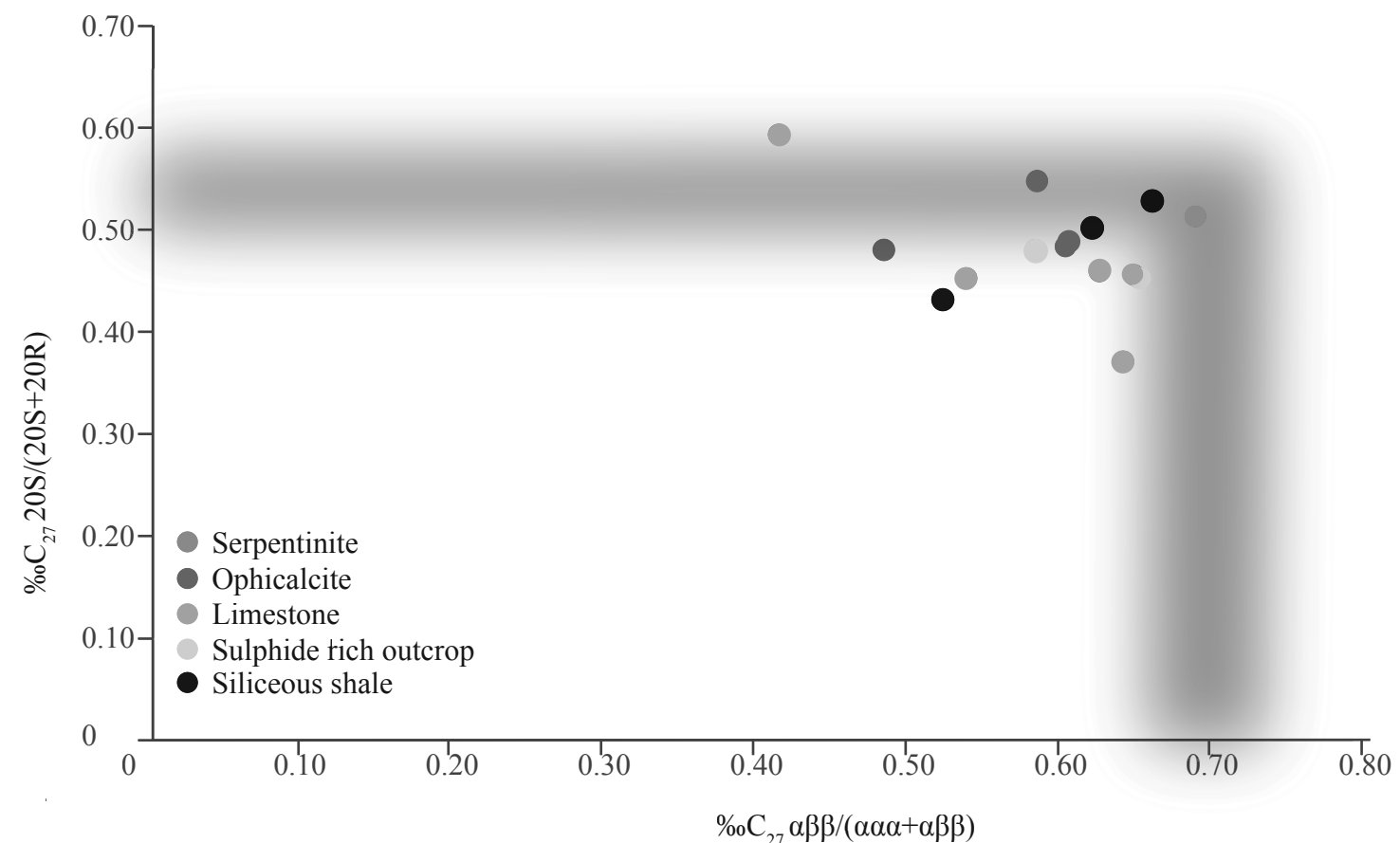


Fig. 6 Thermal maturity parameters of C₂₇ steranes for Totalp samples. The classification is from Peters et al. 2005. The brown shaded area represents the range of complete isomerization for the 20S/(20S + 20R) ααα C₂₇ steranes (ca. 55%) and αββ/(ααα+αββ) C₂₇ steranes (ca. 68%).

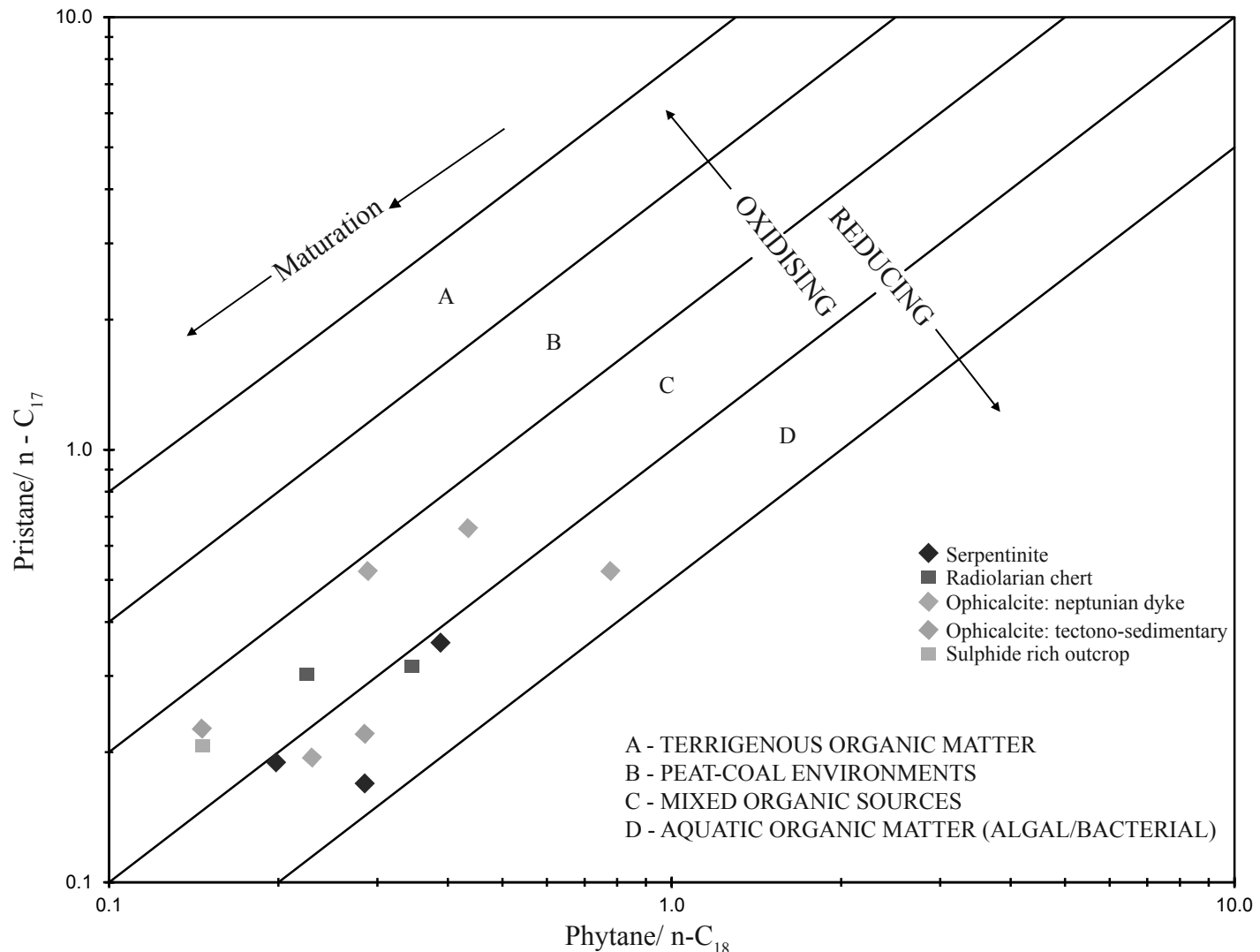


Fig. 7 Plot of pristane/n-C₁₇ vs phytane/n-C₁₈ for Totalp samples used to identify depositional environment and OM type (after Peters et al. 1999).

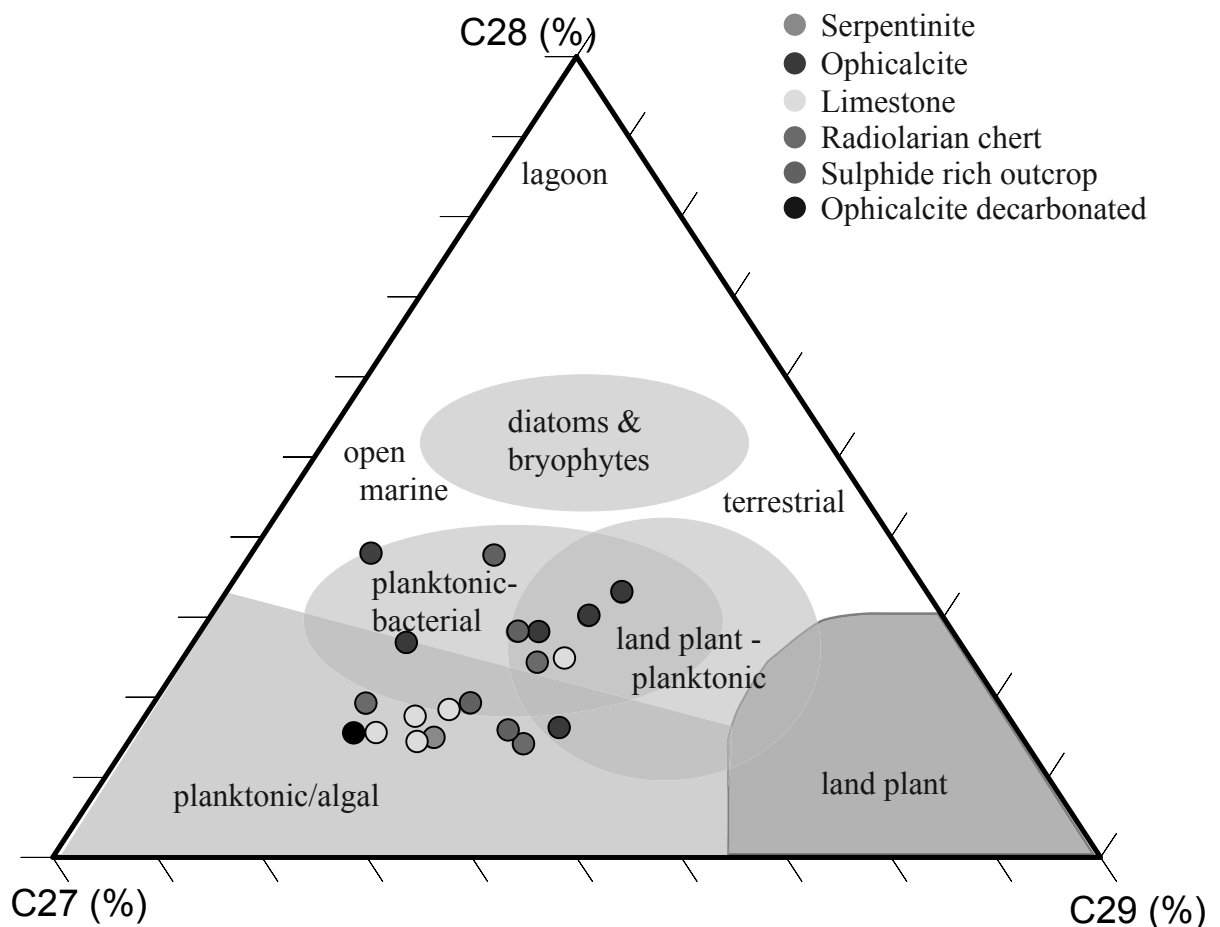


Fig. 8 Sterane ternary distribution of the analysed samples for the $\alpha\beta\beta'$ steranes of Totalp samples. The interpretation of depositional environment is from Patrycja Wójcik-Tabol & Ślączka (2015).

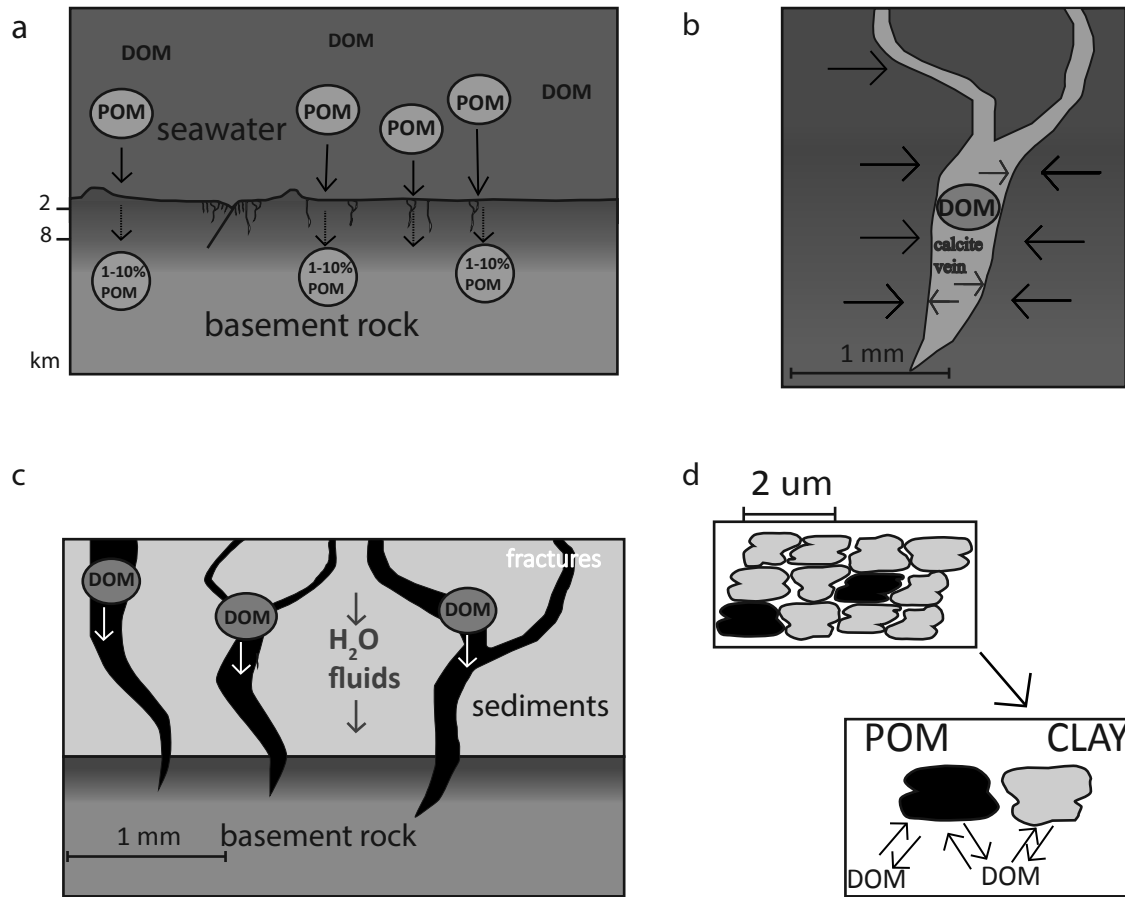


Fig. 9 Conceptual model explaining origin and migration of OM from the seawater into different lithologies in the Totalp unit. **a** The OM is represented by particulate and dissolved organic matter (POM and DOM, respectively). The OM infiltrates the basement rock by rock-fluid circulation. **b** Some OM may be deposited within the carbonate veins (e.g. calcite veins). **c** OM circulates with fluids through fractures and porosity of sediments to migrate into the basement rock. **d** OM is preserved at the surfaces and in the interlayer surfaces of clay minerals in the sedimentary rocks.

Table 1a page 28 Double column Landscape

rock type	sample number	coordinates (UTM)		locality	macroscopic description	mineralogical description	texture	$\delta^{13}\text{C}_{\text{VPDB}}$ (‰) Ca veins	$\delta^{18}\text{O}_{\text{VPDB}}$ (‰) Ca veins
		X (m)	Y (m)						
Serpentinites									
Massive serpentinite	5	561895	5188662	Parsennfurga	massive black serpentinite with white Olivine completely replace by angular borders defining the ex-serpentine minerals, phantoms of peridotite minerals, small green pyroxene, magnetite, later chrysotile veinlets and white carbonate vein; calcite veins with only one stage of crystal growing	mesh ¹	calcite vein, 1 st generation	0.11	-10.2
	16	561522	5188399	2442m. Obersasställi Parsennfurga	Broken serpentinite clasts from a first mainly mesh texture with rare randomly dispersed anhedral magnetite veins crosscut almost perpendicularly by a second generation of white calcite grain; later veins of chrysotile veins	clast supported	calcite vein, 1 st generation	0.03	-11.75
Serpentinite with numerous calcite veins	24	561514	5188009	Obersasställi	generation of greyish deformed calcite ribbon texture;	anhydrite	calcite vein, 1 st generation	0.03	-11.75
	26	561504	5188010	2442m. Obersasställi Parsennfurga	by a second generation of white calcite grain; later veins of chrysotile veins	magnetite	calcite vein, 1 st generation	0.03	-11.75
Red serpentinite	44	561518	5188415	2442m. Obersasställi Parsennfurga	red matrix with dark-black deformed calcite containing also talc and calcite; serpentinite breccia ¹	lizardite	calcite vein, 2 nd generation	1.37	-11.3
	47	561540	5188427	2442m. Obersasställi Parsennfurga	red matrix with numerous calcite veins, also contain dark green the red colour is due to hematite serpentinite.	serpentinite	calcite vein, 2 nd generation	1.37	-11.3
Serpentinite gouge	71	561588	5188095	Obersasställi Parsennfurga	black fine-grained serpentinite with equant serpentine grain following and distributed systematically and fine short veinlets (chrysotile; calcite)	no thin section or XRD	fine grained		
	69	561929	5187152	Obersasställi	black serpentinite with subangular no thin section or XRD serpentinite clasts showing no preferred orientation	no thin section or XRD	fine grained		
Serpentinite cataclasite	70	561929	5187152	Obersasställi	black serpentinite with sub-rounded no thin section or XRD	no thin section or XRD	fine grained		
	77	561482	5187004	Weissfluhjoch	black serpentinite with sub-rounded no thin section or XRD	no thin section or XRD	fine grained		
Massive serpentinite •	78	561482	5187004		anhedral white-grayish peridotite mineral (pyroxene) and small chrysotile veins	no thin section or XRD	no thin section or XRD	no thin section or XRD	no thin section or XRD
						no thin section or XRD	no thin section or XRD	no thin section or XRD	no thin section or XRD
Sedimentary ophiolitic rocks									
Limestone (Neptunian dykes)	1	561543	5188408	2442m. Obersasställi - Parsennfurga	micritic limestone; serpentinite minerals as clasts and veins	pelagic	three types of carbonate crystal rounded to angular coarse grains with hornblend floating randomly in the matrix	porphyro-clastic ¹	calcite vein, 2 nd generation
	23	561514	5188009	Obersasställi					
Tectono-sedimentary ophiolite									
Tectono-sedimentary ophiolite	21	561520	5188015	Obersasställi	red fine carbonate matrix with black serpentinites clasts broken by calcite vein, 1 st generation	with clasts ¹	several generation of carbonate veins; several stage of crystal growing for the carbonates;	calcite vein, 1 st generation	0.32
	25	561511	5188009		anhedral serpentinite broken crosscut by calcite veins			calcite vein, 1 st generation	0.58
	39	561515	5188439	2442m. Obersasställi - Parsennfurga				calcite vein, 2 nd generation	1.78
	41	561572	5188406					calcite vein, 1 nd and 2 nd gener.	0.42 ; 1.07
	42	561572	5188406					calcite vein, undetermined	-10.3 ; -8.6
	46	561540	5188418					generation	-6.2
	66	564260	5190402	near Grüenhorn					

rock type	sample number	coordinates (UTM)		locality	macroscopic description	mineralogical description	texture	Carbonate texture	$\delta^{13}\text{C}_{\text{VPDB}}$ (‰) Ca veins	$\delta^{18}\text{O}_{\text{VPDB}}$ (‰) Ca veins
		X (m)	Y (m)							
Reworked tec-sed. ophicalcite	9	562586	5188578	Parsennfurga- Parsennhütte	pink carbonate with randomly orientated elongated clast of ophicalcite (serpentinite+carbonate); calcite veins	no thin section or XRD	reworked ¹			
Vein supported serpentinite breccia	72	561929	5187152	2442m. Obersasställi - Parsennfurga	centimetric angular clasts of green serpentinite tectonically broken by calcite veins	no thin section or XRD	vein supported breccia	calcite vein, undetermined generation	1.60	-10.6
Sediments										
Radiolarite	62	564212	5190386	near Grünenhorn from sulphide rich outcrop	hard fine grained red siliceous rock ; post deposition quartz vein perpendicular to the geometry of deposition	no thin section or XRD	fine grained	post-deposit calcite vein	- 0.79	-6.4
	68	564252	5190393							
Siliceous shale	60	564212	5190386	near Grünenhorn from sulphide rich outcrop	greyish - reddish fine grained siliceous rock, great porosity and numerous fractures	composed mainly by quartz (46%), plagioclase(30%), chlorite, muscovite and hematite	fine grained			
	61	564212	5190386							
	15	564049	5189517	Gotschnagrat	red and grey fine grained intercalated siliceous shale with deformed quartz veins	dominated by quartz (89%) with plagioclase, muscovite, chlorite and trace of hematite	fine grained			
	18	564213	5189544							
Limestone	10	562494	5188558	Parsennfurga- Parsennhütte	grey limestone with numerous calcite veins of two generation perpendicular to each other	pelagic limestone, evidence of almost fossil organisms filled by sparry calcite	fine grained			
	19	563790	5189694	Gotschnagrat						
Limestone	53	563144	5188716	south from Parsennhütte	grey limestone with fine greyish veins and rare short calcite veins with pink pelagic limestone (hematite) in places	no thin section or XRD	fine grained			
	54	563140	5188707							
	56	563140	5188707							
	57	563144	5188716							
	58	563144	5188716							
Carbonate (Sulphide rich outcrop)	63	564212	5190386	near Grünenhorn	carbonate rock with deformed quartz veins; microscopic grain of pyrite everywhere except in the quartz and calcite veins	dominated by calcite (53%) with porphyro-clastic				
	64	564212	5190386							
	65	564252	5190393		very fractured sample with greater porosity					

Table 1. Results by lithology including mineralogy and texture observed in hand specimens and the texture on the calcites used for the isotopic analyses ($\delta^{13}\text{C}_{\text{VPDB}}$ and $\delta^{18}\text{O}_{\text{VPDB}}$). The vein generation is defined from the specific example and may not correlate across all samples. ¹ Thin section of the lithology is observed. • All lithology are from the lower sub-unit with the exception of the massive serpentinite (samples 77, 78).

Table 2 page 30

Double column Landscape

	sample number	Total Carbon ppm	Total C _{organic} ppm	Hydrocarbons (HC) ppm	n-alkanes			$\delta^{13}\text{C}_{\text{VPDB}}$ (‰) on TOC	Steranes	Hopanes	PAH ^{s•}
					Range	C _{max}	CPI				
Serpentinite											
Massive serpentinite	5, 16	395- 3135	102 - 176	23-900	16-39	C ₂₀ , C ₂₉	0.76 - 1.29	20 - 28	BDL	BDL	*
Serpentinite with numerous Ca veins	24, 26, 44, 47	20400-42500	19 -135	1 - 124	16 - 35	C ₂₀ , C ₂₆	0.8 - 1.05	22 - 28	BDL	BDL	*
Red serpentinite (with hematite)	71	88205	268	1	17-35	C ₂₆	1.17	22.3	BDL	BDL	**
Serpentinite gouge	69	539	284	3	17-33	C ₂₉	0.94	26.0	BDL	*	BDL
Serpentinite cataclasite	70	876	269	46	17-36	C ₂₀	0.94	24.1	BDL	BDL	**
Massive serpentinite ¹	77, 78	454	≈190	0.05-4	17-40	C ₂₉	0.84 - 0.97	29 - 30	BDL	*	BDL
Ophicalcite											
Neptunian dykes	1, 23	95600 - 107500	15 - 103	0.03 - 121	17 - 35	C ₂₉	1.05	27 - 29	- 27.06	**	**
Tectono-sedimentary ophicalcite											
Red matrix, serp. claste and Ca veins	21, 25, 39, 41, 42, 46, 66	33360 - 101700	11 - 116	2 - 2470	17-38	C ₁₈ to C ₂₈	0.81 - 1.42	23 - 31	-27.4	**	**
Reworked tec-sed. Ophicalcite	9	106000	86	50	16-36	C ₂₂	0.65	24	-26.1	BDL	*
Serp-clasts in Ca veins	72	69600	30	124	20-36	C ₂₉	0.90	28	BDL	BDL	BDL
Sediments											
Radiolarite from sulphide rich outcrop	62, 68	671 - 13200	66-187	1 - 17	17 - 34	C ₂₀ , C ₃₁	1.19-2.87	24 - 28	BDL	***	*
Siliceous shale from sulphide rich outcrop	60, 61	384 - 672	194 - 433	22-144	16 - 37	C ₂₀ , C ₂₇	1.05 - 1.52	23 - 25	**	**	**
Siliceous shale near sulphide rich outcrop	15, 18	285- 318	136- 145	13 - 27	16-33	C ₁₈ , C ₂₀	0.95 - 1.19	23 - 24	*	*	BDL
Limestones	10,19	98200 - 129000	74- 82	79 - 171	16-35	C ₂₂ , C ₂₇	0.92 - 0.94	23 - 27	- 26.62	BDL	****
Limestone from Parseennhütte	53, 54, 56, 57, 58	46500 - 94500	14 - 92	3 - 238	16 - 37	C ₂₃ , C ₂₉	0.82 - 1.10	22 - 23	*	*	***
Sulphide rich outcrop	63, 64, 65	442 - 90400	153 - 647	1 - 24	17-33	C ₂₀ , C ₂₇	0.93- 1.55	23 - 26	- 26.02	**	**

Table 2. Results by lithology including TC, TOC and total HC concentration in ppm (parts per million) and organic carbon isotopic composition of bulk rock $\delta^{13}\text{C}_{\text{VPDB}}$ organic. For the n-alkanes: the carbon number range (n-alkanes range), the maximum carbon number (Cmax), carbon preference index (CPI values) and mean carbon number (MC#) are shown. For the steranes, hopanes and PAHs the concentrations are in ppm and are represented in intervals by star symbol *, where * = [0 - 0.1], ** = [0.1 - 1] and *** = [1 - 10] and BDL = below detection limit. a: identified PAHs in the samples were: Phenanthrene, P; Fluoranthene, Fluo; Pyrene, Pyr; Chrysene, Chry; Benzo(a)anthracene, BaA; Benzo(b)fluoranthene, BbF; Benzo(a)pyrene, BaP; Indeno(1,2,3-cd)pyrene, IndPy; Benzo(ghi)perylene, BghiP; Dibenzothiophene (DBT), methylP (3,2,1 and 9 MPs) and 2-methyl naphthalene ; not all were present in every sample.¹ All lithology are from lower sub-unit except the massive serpentinite (samples 77, 78) which is from upper sub-unit



Click here to access/download

Supplementary Material

alphabetical glossary Mateeva et al page 31.docx

